Contrib Mineral Petrol (2006) 151: 222–242
DOI 10.1007/s00410-005-0056-1

ORIGINAL PAPER

Cin-Ty Aeolus Lee · Xin Cheng · Ulyana Horodyskyj

The development and refinement of continental arcs by primary basaltic magmatism, garnet pyroxenite accumulation, basaltic recharge and delamination: insights from the Sierra Nevada, California

Received: 3 May 2005 / Accepted: 30 November 2005 / Published online: 13 January 2006

Abstract The lower crust of the Mesozoic Sierra Nevada batholith was made up of high MgO, garnet-poor and low MgO, garnet-rich pyroxenites. Both groups are genetically linked and are collectively complementary to the mafic to intermediate Sierran plutons. High MgO pyroxenites represent high pressure cumulates from a mantle-derived hydrous basalt or basaltic andesite, resulting in derivative magmas having unusually low MgO for a given SiO_2 as represented by the numerous mafic enclaves found in many Sierran plutons. The low MgO pyroxenites are either (1) shallow pressure cumulates from these derivative magmas or (2) partial melting residues (restites) of these derivative magmas after they were emplaced and solidified at lower crustal levels. In both cases, the complementary melt to the low MgO pyroxenites is driven to higher SiO_2 contents, generating diorites and granodiorites. However, this simple two-stage scenario for the origin of Sierran granitoids cannot explain the observation that the Mg# of Sierran intermediate magmas remains roughly constant at ~0.45–0.50 with increasing SiO_2. Basaltic recharge/mixing with the lower crust is suggested as one means of buffering Mg#s and re-melting the lower crust to generate granitic melts, the latter of which mix with more juvenile magmas to complete the Sierran differentiation series.

Introduction

The continental crust, defined vertically as that part of continents lying above the seismic Moho discontinuity and laterally as that bound by continental shelves, is a significant repository for highly incompatible trace elements in the bulk Earth. In contrast, the upper portions of the Earth's mantle appear to be depleted in these same elements, which has led to the widely held view that the upper part of the mantle is simply the complementary residue of continental crust extraction (Hofmann 1988). The problem, however, is that in terms of major elements, the average composition of the continental crust is too felsic (SiO_2~60 wt. %) to have been directly derived from the ultramafic lithologies (peridotite) believed to dominate the mantle (Kay and Kay 1988; Rudnick 1995)– melting of a peridotite generates basalt and hence mafic compositions ($SiO_2 < 50$ wt. %). Indeed, oceanic plateaus and integrated crustal columns in island arcs, both of which have been proposed to be the building blocks of continental crust, are basaltic (DeBari and Sleep 1991; Miller and Christensen 1993; Fliedner and Klemperer 1999). This discrepancy forms the essence of the well-known "continental crust paradox" (Kay and Kay 1988; Kelemen 1995; Rudnick 1995). What this means is that if continental crust can be ultimately traced back to a peridotitic mantle source, a missing mafic to ultramafic reservoir is needed to balance the composition of the felsic crust with respect to a basaltic parent (Kay and Kay 1988, 1993).

A number of hypotheses have been put forward to reconcile the apparent paradox. The common feature of most hypotheses is that the basaltic parent material must be differentiated into complementary felsic and mafic components, followed by physical separation of the mafic component from the continental crust, driving what remains of the continental crust towards felsic compositions (in some models, the parental magma could be a magnesian andesite; Kelemen et al. 2003). One scenario for the formation of felsic continental crust is via arc magmatism (Arndt and Goldstein 1989; Kay and Kay 1993; Tatsumi 2000; Kelemen et al. 2003). In this scenario, fractional crystallization of a basaltic magma at depth generates a gabbroic or garnet pyroxenitic cumulate (depending on pressure), both of which are mafic to ultramafic in composition. If accumulation

Communicated by T. L. Grove

C.-T. A. Lee (✉) · X. Cheng · U. Horodyskyj
Department of Earth Science, MS-126, Rice University,
6100 Main Street, Houston,
TX 77005, USA
E-mail: ctlee@rice.edu
Tel.: +1-713-3485084

occurs at great enough depths or if the cumulate pile is subsequently depressed into the garnet stability field, a layer of garnet pyroxenite would form at the base of the continental crust. Because of the high density of garnet pyroxenite relative to peridotitic mantle, these cumulate piles will eventually become negatively buoyant and may perhaps founder or delaminate (this term is used loosely here to describe any removal of lithosphere; no specific mechanism is implied) back into the upper mantle (Conrad and Molnar 1997; Jull and Kelemen 2001; Morency and Doin 2004). The number of geophysical and geochemical observations being interpreted to be associated with delamination has increased dramatically in the last two decades. For example, evidence for delamination has been suggested beneath the Mesozoic Sierra Nevada batholith in California (Zandt and Carrigan 1993; Jones et al. 1994; Ducea and Saleeby 1996; Wernicke et al. 1996; Zandt et al. 2004), the Alboran Sea in the western Mediterranean (Seber et al. 1996), and the Altiplano in the active Andean arc (Kay and Kay 1993).

Evidence for delamination, however, does not mean that the "crustal paradox" is solved. What is missing is the nature of the differentiation process that leads to the formation of a mafic lower crust. It is thus necessary to find these putative garnet pyroxenitic lithologies and assess how they might balance the composition of the continental crust with respect to a basaltic parent. However, the delamination hypothesis predicts that any putative reservoirs should in general be missing, making the hypothesis difficult to test from the outset. Here, we investigate garnet pyroxenite xenoliths from the Sierra Nevada, California. Many of these samples are more mafic than basaltic melts and thus at face value represent reasonable candidates for the hypothesized missing mafic component. Ducea and Saleeby (1996) showed that these garnet pyroxenite xenoliths are present in late Miocene alkali basalts erupted through the Sierra Nevada, but are entirely absent from Late Pliocene volcanic centers. The simplest interpretation of this temporal change in xenolith demographics is that, prior to the Miocene, the Sierra Nevada was underlain by a thick garnet pyroxenitic root associated with Mesozoic arc formation (Ducea and Saleeby 1996). Some time in the Pliocene, this root probably foundered and was replaced by asthenospheric mantle (Jones et al. 1994; Ducea and Saleeby 1996, 1998a; Wernicke et al. 1996; Lee et al. 2000, 2001; Manley et al. 2000; Ducea 2001, 2002; Farmer et al. 2002; Boyd et al. 2004; Zandt et al. 2004). The Sierran garnet pyroxenites may thus represent a fortuitous snapshot of mafic lower crust prior to delamination.

Here, we build on the work of Ducea and Saleeby (1996) by showing that the Sierran garnet pyroxenites can be subdivided into two distinct but petrogenetically related groups based on bulk composition and mineralogy. The recognition of two pyroxenite groups is shown here to be fundamentally important in understanding the origin and evolution of Sierran mafic to intermediate plutons.

Samples and methods

Samples

Garnet pyroxenites are found in late Miocene alkali basalts erupted through the central Sierra Nevada. The samples examined here were collected from an 8.3 Ma plug near Big Creek (see Dodge et al. 1988 for latitude and longitude coordinates). The petrography and thermobarometry of such pyroxenites have been investigated in several earlier studies (Dodge et al. 1988; Mukhopadhyay and Manton 1994; Ducea and Saleeby 1996, 1998b). Although considerable isotopic work has been done on the pyroxenites, there has only been limited discussion of their whole-rock major and trace-element geochemistry (Ducea 2002). Here, we combine six samples described in Ducea (2002) with 13 new samples presented here. Spinel peridotites and garnet-bearing spinel peridotites also occur at this xenolith locality and have been extensively described by Lee and co-workers (Lee et al. 2000,2001; Lee 2002).

Methods

Depending upon how much sample was available, major-element compositions of garnet pyroxenites were determined by X-ray fluorescence spectroscopy (XRF; Washington State University at Pullman), inductively coupled plasma mass spectrometry (ICP-MS), or by reconstruction using mineral chemistries (electron microprobe analysis) and mineral modes (estimated from point counting). Major element compositions are shown in Tables 1 and 2. Trace-element compositions were determined by ICP-MS although some elements were also determined by XRF for comparison. Samples were crushed and powdered in a ceramic disk mill (Spex) that was free from metal contamination. For ICP-MS, 50–80 mg aliquot of sample powder was dissolved overnight in a mixture of 0.25 mL of HF with 0.25 mL $HClO_4$ at 140°C in a sealed wrench-top 2.5 mL Teflon beaker. This was followed by open-air dry down at 175°C in a percholoric fume hood. This dissolution-dry down procedure was repeated once more. Afterwards, the contents of the beaker were diluted into 125 mL of 2 wt. % HNO_3, yielding a dilution factor of ~2000. Indium tracer was added to the solution to yield roughly a 1 ppb in concentration. The diluted solutions were introduced into a ThermoFinnigan Element 2 ICP-MS at Rice University. Indium was used as an internal standard to correct for instrumental drift. Rock standards BHVO-1 (Hawaiian basalt) and BIR-1 (Icelandic basalt) were used as external standards by processing them through the same procedure as the samples. These two standards have similar major-element matrices to the Sierran garnet pyroxenites but importantly have high and low contents of incompatible trace elements, respectively, allowing us to bracket the range seen in the

Table 1 Major element compositions

	Low MgO garnet pyroxenite							High MgO garnet pyroxenite					
	BC98-9 Gt-Cpx	BC52 Gt-Cpx	BCX Gt-Cpx	BC49 Gt-Cpx	1026S Gt-Cpx	1026P Gt-Cpx	1026R Gt-Cpx	BC76 Gt-Cpx	BC41 Gt-Cpx	BC98-5 Gt-Cpx	BC72 Gt-Cpx	BC98-7 Gt-Web	BC98-1 Gt-Web
XRF													
SiO_2	42.70	41.85	45.17					49.11	48.90	49.34	49.80	49.55	48.43
Al_2O3	9.81	16.93	15.11					7.67	7.69	7.45	6.68	8.53	10.13
TiO_2	0.42	1.70	0.40					0.75	0.49	0.61	0.54	0.37	0.49
FeOT	13.19	13.86	13.55					8.83	8.36	9.44	8.94	11.31	11.88
MnO	0.52	0.25	0.30					0.16	0.15	0.19	0.17	0.22	0.22
CaO	26.09	13.59	12.70					15.43	12.92	12.84	13.53	8.09	6.28
MgO	4.33	8.77	9.81					15.58	17.77	17.56	18.63	20.04	20.67
K_2O	0.03	0.16	0.41					0.23	0.42	0.06	0.15	0.10	0.12
Na_2O	0.69	0.92	1.39					1.09	1.22	0.70	0.57	0.69	0.63
P_2O_5	0.22	0.69	0.11					0.02	0.02	0.01	0.02	0.01	0.01
Total	98.00	98.72	98.95					98.86	97.95	98.19	99.03	98.90	98.87
Mg#	0.37	0.53	0.56					0.76	0.79	0.77	0.79	0.76	0.76
Reconstructed (Electron microprobe)													
SiO_2		43.73	46.99		43.86	48.03	41.37	50.39	48.92	50.62	50.82	49.91	47.53
Al_2O_3		16.56	14.95		17.75	11.06	18.61	7.53	8.30	7.72	7.46	8.10	12.62
TiO_2		0.19	0.11		0.13	0.11	0.20	0.11	0.81	0.04	0.12	0.05	0.07
Cr_2O_3		0.06	0.01		0.02	0.04	0.06	0.04	0.26	0.07	0.17	0.09	0.14
FeOT		14.37	13.12		13.67	11.55	13.84	7.24	6.12	8.50	6.85	9.20	12.56
MnO		0.39	0.35		0.35	0.18	0.38	0.15	0.11	0.21	0.20	0.21	0.32
CaO		13.80	13.36		12.75	13.92	10.69	18.35	17.14	15.22	18.43	11.96	7.61
MgO		10.22	9.55		11.23	12.45	13.20	14.26	15.26	16.65	14.89	18.31	18.46
Na_2O		0.40	1.63		0.75	1.28	0.46	1.27	1.53	0.79	0.57	0.80	0.41
Total		99.72	100.1		100.51	98.62	98.80	99.34	98.45	99.82	99.50	98.65	99.71
Mg#		0.56	0.56		0.59	0.66	0.63	0.78	0.82	0.78	0.80	0.78	0.72
ICPMS													
Al_2O_3	8.71	16.14	14.78	19.79				7.33	7.13	7.50	6.46	8.51	9.96
TiO_2	0.402	1.653	0.406	0.386				0.796	0.479	0.617	0.609	0.418	0.518
FeOT	12.07	12.85	12.68	12.88				8.81	8.23	9.47	8.74	11.20	11.89
MnO	0.459	0.227	0.276	0.306				0.148	0.142	0.178	0.162	0.210	0.217
CaO	23.23	12.35	12.07	10.36				14.87	11.89	12.34	13.52	7.97	6.07
MgO	3.90	8.30	9.42	11.49				15.43	17.49	17.90	18.02	19.56	20.54
K_2O		0.11	0.40	0.21				0.19	0.34		0.14	0.06	0.08
P_2O_5	0.219	0.672	0.111	0.018				0.016	0.015	0.010	0.009	0.009	0.012
Mg#	0.37	0.54	0.57	0.61				0.76	0.79	0.77	0.79	0.76	0.75

garnet pyroxenites. Calibration values are taken from Eggins et al. (1997). Procedural blanks were subtracted from all samples. Rock standards AGV-1 (andesite) and JP1 (peridotite) were treated as samples to monitor quality. For most trace-elements, ICP-MS analyses were conducted under low mass resolution mode (where sensitivity is highest), that is, $m/\Delta m = 300$. For major elements and low mass elements that are complicated by various molecular interferences, we used the medium resolution option on the ICP-MS ($m/\Delta m = 3{,}000$). In these cases, magnetic drift was corrected for by locking onto the Ar dimer. Systematic offsets due to magnet hysteresis were corrected for empirically using the 'mass offset' option. Zr and Hf concentrations of the pyroxenites were also measured by isotope dilution. Isotope dilution measurements follow the same wet chemistry procedure as described above, but instead of using an external standard, a mixed-tracer solution containing calibrated quantities of enriched Zr (^{94}Zr) and Hf (^{180}Hf) was used.

Electron microprobe measurements were done in wave-length dispersive mode on JEOL JXA-8600 at the Texas Center for Superconductivity and Advanced Materials at the University of Houston. Olivine, pyroxene and garnet standards were used for external calibration.

Results

Sierran garnet pyroxenites

Petrologic and geochemical distinctions

The garnet pyroxenites are dominated by clinopyroxene and garnet with lesser amounts of orthopyroxene, occasional amphibole, and accessory phases, such as rutile, Fe–Ti oxides, and apatite. There is no evidence for olivine in any of the pyroxenite samples selected for this study. Clinopyroxenes and orthopyroxenes both show an extensive pyroxene exsolution lamellae. Exsolution lamellae of garnet in both pyroxenes are also seen. Garnet exsolution lamellae have also been seen in garnet peridotites from the same xenolith suite (Lee et al. 2001).

Table 2 Mineral chemistries from electron microprobe measurements

	BC52		BCX		1026S		1026P			1026R		BC49		BC76	
Mode	Cpx 34	gt 67	cpx 50	gt 50	cpx 30	gt 70	cpx 50	gt 40	amph 10	cpx 23	gt 77	cpx 44	gt 56	cpx 79	gt 21
SiO_2	51.19	39.97	54.42	39.56	53.70	39.65	54.66	39.51	48.95	51.85	38.24		41.22	52.86	40.87
TiO_2	0.34	0.12	0.14	0.08	0.15	0.12	0.10	0.06	0.34	0.12	0.22		0.09	0.12	0.09
Al_2O_3	4.56	22.61	7.50	22.41	5.06	23.18	3.77	20.93	8.07	4.31	22.88		23.54	3.50	23.06
Cr_2O_3	0.15	0.01	0.01	0.00	0.03	0.02	0.03	0.05	0.02	0.07	0.05		0.01	0.02	0.15
FeO	4.62	19.27	5.69	20.54	3.64	17.97	4.11	21.36	9.52	3.03	17.07		15.94	4.27	18.69
MnO	0.25	0.46	0.08	0.63	0.03	0.49	0.03	0.41	0.09	0.04	0.48		0.48	0.05	0.51
NiO	0.18	0.01	0.01	0.00	0.00	0.00	0.03	0.03		0.03	0.01		0.01	0.17	0.00
MgO	14.64	8.00	11.57	7.54	13.59	10.22	13.30	9.76	18.97	14.93	12.68		9.96	14.85	12.00
CaO	21.39	9.98	17.54	9.18	21.10	9.17	21.17	6.44	7.54	21.93	7.34		8.29	21.75	5.24
Na_2O	1.13	0.03	3.24	0.02	2.44	0.02	2.31	0.02	1.15	1.90	0.03		0.33	1.59	0.02
Total	98.44	100.47	100.19	99.96	99.74	100.84	99.51	98.57	94.65	98.21	98.99		99.87	99.18	100.64
Mg#	0.85	0.43	0.78	0.40	0.87	0.50	0.85	0.45	0.78	0.90	0.57		0.53	0.86	0.53
TEG (1.5 Gpa)	756°C		831°C		771°C		695°C			724°C				740°C	
Density (g/cm3)	3.737		3.626		3.705		3.600			3.746				3.458	
Vp (km/s)	8.501		8.445		8.590		8.287			8.632				8.065	
Vs (km/s)	4.861		4.829		4.908		4.727			4.924				4.604	

	BC41		BC98-5			BC72			BC98-7				BC98-1		
Mode	cpx 57	gt 3	cpx 61	gt 25	opx 14	cpx 74	gt 26	opx 0	cpx 48	gt 27	opx 25	Amph 0	Cpx 23	gt 50	opx 27
SiO_2	53.89	41.06	53.14	40.96	56.88	54.37	40.73	56.69	52.48	41.11	54.48	42.46	52.61	41.28	54.93
TiO_2	0.18	0.07	0.07	0.01	0.00	0.11	0.13	0.01	0.09	0.04	0.00	1.75	0.11	0.08	0.02
Al_2O_3	2.76	22.92	3.02	22.93	0.94	2.10	22.70	1.79	3.14	23.15	1.40	14.89	2.83	23.18	1.13
Cr_2O_3	0.21	0.37	0.01	0.23	0.04	0.12	0.28	0.06	0.01	0.31	0.01	0.32	0.10	0.21	0.03
FeO	3.93	17.15	3.72	17.95	12.16	3.46	16.50	11.03	3.43	16.70	12.13	8.29	4.01	16.91	11.74
MnO	0.07	0.54	0.06	0.61	0.13	0.06	0.60	0.14	0.05	0.53	0.15	0.14	0.18	0.50	0.12
NiO	0.02	0.00	0.27	0.00	0.04	0.03	0.00	0.06	0.40	0.01	0.11	0.06	0.28	0.00	0.06
MgO	15.18	12.84	15.76	11.77	28.99	15.51	13.15	29.66	15.28	12.40	30.40	15.52	16.51	12.70	31.08
CaO	22.32	5.55	22.80	5.50	0.17	22.89	5.73	0.20	21.79	5.42	0.34	10.76	21.00	5.37	0.22
Na_2O	0.84	0.01	1.15	0.36	0.01	0.75	0.04	0.01	1.52	0.25	0.03	2.62	1.22	0.24	0.02
Total	99.40	100.52	100.00	100.31	99.34	99.39	99.86	99.64	98.19	99.91	99.05	96.79	98.84	100.47	99.34
Mg#	0.87	0.57	0.88	0.54	0.81	0.89	0.59	0.83	0.89	0.57	0.82	0.77	0.88	0.57	0.83
TEG (1.5 Gpa)	760°C		701°C			739°C			719°C				740°C		
PBKN-TBKN			1.1 Gpa – 576°C			1.2 Gpa – 734°C			0.6 Gpa – 561°C				2.9 Gpa – 901°C		
PBKN-TEG			1.9 Gpa – 713°C			1.2 Gpa – 730°C			1.4 Gpa – 714 C				2.0 Gpa – 756°C		
PBKN-TH			1.8 Gpa – 689°C			1.0 Gpa – 681°C			1.2 Gpa – 694°C				1.7 Gpa – 698°C		
Twells			727°C			832°C			704°C				899°C		
Density (g/cm3)			3.473			3.454			3.477				3.478		
Vp (km/s)			8.083			8.093			8.111				8.102		
Vs (km/s)			4.642			4.625			4.680				4.677		

gt Garnet, *opx* orthopyroxene, *cpx* clinopyroxene, *amph* amphibole, *TEG* Fe–Mg exchange between garnet and clinopyroxene (Ellis and Green 1979), *PBKN* Al in orthopyroxene coexisting with garnet (Brey and Kohler 1990), *TBKN* Fe–Mg exchange between orthopyroxene and clinopyroxene (Brey and Kohler 1990), *TH* Fe–Mg exchange between garnet and orthopyroxene (Harley 1984), *TWells* Fe–Mg exchange between orthopyroxene and clinopyroxene (Wells 1977), *Vp* compressional velocity at STP conditions, *Vs* shear velocity at STP conditions

Rutiles occur predominantly as euhedral amber-colored grains, but also occasionally as exsolution products from garnet. In most cases, Fe–Ti oxides are associated with rutile and occur as opaque rims or opaque lamellae.

Whole-rock major and minor element data determined by XRF and ICP-MS are shown in Table 1. Major and minor element chemistries of garnet and pyroxenes are shown in Table 2. We have combined mineral chemistries with mineral modes determined by point counting (Table 2) to reconstruct the major and minor element compositions of the pyroxenites. It can be seen in Table 1 that reconstructed and measured whole-rock compositions agree very well for major elements and some minor elements (Na_2O). However, for TiO_2, reconstructed values are systematically less than that of the measured whole-rock values. This is due to the presence of rutile and Fe–Ti oxides, which were not factored into the reconstruction. Assuming that all the "missing" TiO_2 is associated with rutile (and that Fe–Ti oxides have mostly exsolved from rutile or represent reactions between rutile and the silicate matrix), we estimate the weight concentration of rutile in all samples to be less than 0.6% (with the exception of BC52, which could have 1.5 wt. % rutile).

Based on these major element compositions and modal mineralogies, the Sierran garnet pyroxenites can

be subdivided into two distinct geochemical and petrologic groups (Figs. 1, 2) even though they have been previously treated as one group (Ducea 2002). The Sierran garnet pyroxenites are represented by a high MgO (>15 wt.%) and a low MgO (<15 wt.%) group (Figs. 1, 2a). The high and low MgO groups do not represent a compositional continuum as seen in Fig. 2. The former is dominated by clinopyroxene (>50%) with lesser amounts of garnet and some orthopyroxene; both garnet websterites (garnet + clinopyroxene + orthopyroxene) and garnet-poor clinopyroxenites are represented by this group. The low MgO group, in contrast, contains garnet, clinopyroxene and occasional amphibole and plagioclase but no orthopyroxene. Unlike the high MgO group, garnet mode is >50% in the low MgO group. Both groups have been referred to in the literature as "eclogites", but strictly speaking should be referred to as garnet pyroxenites or clinopyroxenites because the clinopyroxenes are not particularly omphacite rich (Mukhopadhyay and Manton 1994).

Additional differences in the major element compositions of the two groups are as follows. The high MgO group is characterized by bulk SiO_2 contents generally between 45–52 wt. %, Al_2O_3 contents less than ~10 wt. % and Mg#s (molar Mg/(Mg + Fe)) between 0.75–0.82 (Fig. 2a–d). The low MgO group is characterized by SiO_2 contents <45 wt. %, and Al_2O_3 contents >10 wt. %. There is no obvious distinction between the two groups in terms of FeO, Na_2O, and CaO contents (Figs. 2b,e,f). The higher SiO_2 and lower Al_2O_3 content of the high MgO group is a manifestation of its more pyroxene-rich and garnet-poor nature compared to the low MgO group (pyroxene is Si-rich and Al-poor compared to garnet). Although, this may suggest that the gross compositional differences between the two pyroxenite groups may be artifacts of metamorphic segregation of a garnet pyroxenite into garnet-rich and pyroxene-rich zones, the bulk compositional differences are demonstrably real. This is evidenced by the observation that mineral chemistries of garnets and clinopyroxenes also differ between each group. For example, in Fig. 3a, b, it can be seen that clinopyroxenes from the high MgO group have high MgO and low Al_2O_3 contents compared to those from the low MgO group. Similarly, garnets from the high MgO group have higher MgO and lower CaO contents.

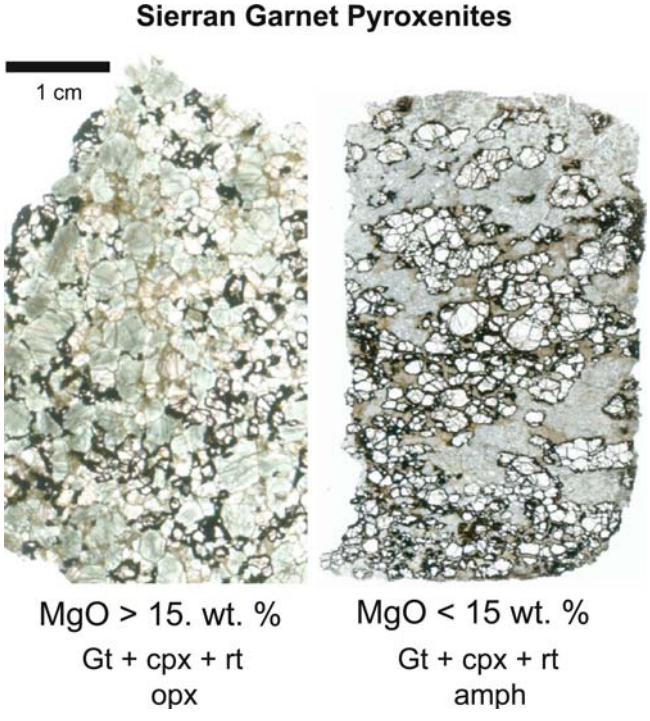

Fig. 1 Representative thin sections of the high (>15 wt. % MgO) and low (<15 wt. %) MgO pyroxenites

The two pyroxenite groups are further distinguished by their trace element compositions. The high MgO group has distinctly higher Ni and Cr contents than the low MgO group (Fig. 4). The very high Cr contents in the high MgO group are undoubtedly due to the higher clinopyroxene mode as Cr is known to be compatible in clinopyroxene. Combined with their characteristically high Mg#s, the high Ni and Cr contents of the high MgO group indicates that the high MgO group is more primitive than the low MgO group. Another important distinction between the two pyroxenite groups is that the heavy rare-earth element (HREE) contents of the low MgO group are higher than that of the high MgO group (Figs. 5a,b). In particular, some of the low MgO garnet pyroxenites are characterized by HREE enrichments relative to the light rare earth elements (LREEs), consistent with the higher abundance of garnet in this group and requiring that garnet was a primary magmatic phase (LREE enrichments may be due to the late stage metasomatism and/or contamination from the host lava and are hence ignored; (Lee 2005)). In contrast, the lack of pronounced HREE enrichment in the high MgO group is consistent with the lower abundance of garnet in this group. Garnet may or may not have been present as a primary magmatic phase in the high MgO pyroxenites. The flat HREE abundance patterns suggest that small amounts of garnet may have been present as a magmatic phase. However, given the similarity of HREE abundances with garnet-free gabbroic cumulates (Fig. 5), it is more likely that most of the garnet present in the high MgO group exsolved from pyroxenes, a feature that would be consistent with the textural evidence (see above).

Temperatures and pressures of equilibration

One question that arises is whether the two pyroxenite groups derive from different depths in the lithosphere. Suitable barometers exist only for those assemblages containing orthopyroxene and garnet (Harley and Green 1982; Brey and Kohler 1990). For those samples containing orthopyroxene (some of the high MgO pyroxenites), we obtain equilibration pressures between

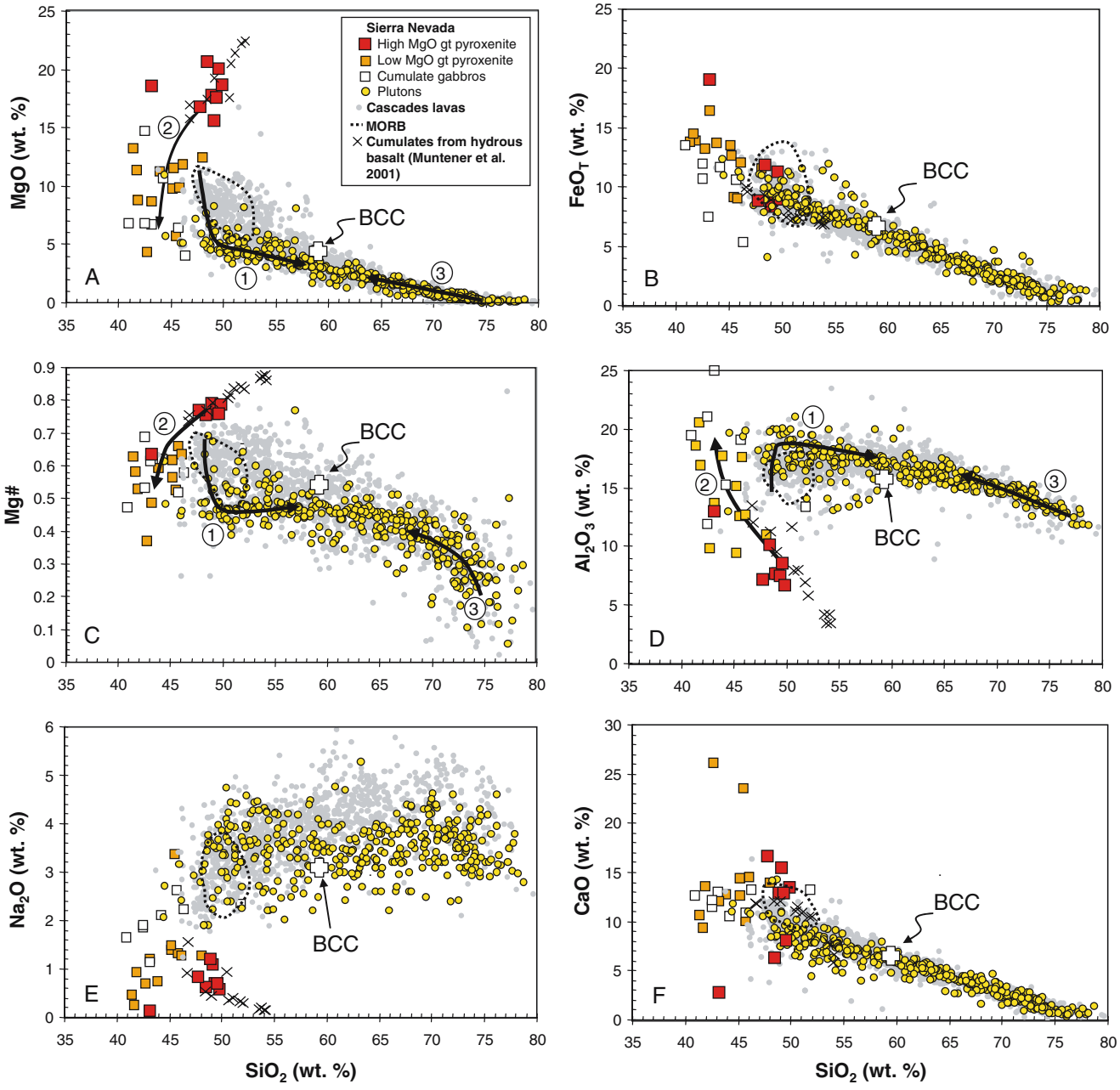

Fig. 2 Variation diagrams illustrating geochemical relationships between Sierra Nevadan garnet pyroxenites (this study), Sierran cumulate gabbros (Sisson et al. 1996), cumulate compositions from high pressure crystallization experiments of hydrous basalts and basaltic andesites (Müntener et al. 2001), Sierran mafic to felsic plutons (see text for data sources), and Cascades arc lavas (from GEOROC database). *Dashed outlined region* represents field for mid-ocean ridge basalts from RidgePetDB (Lehnert et al.2000). Sierran magmas are interpreted to represent the products of a mature arc, whereas the *Cascades arc* is taken to represent a juvenile or incipient arc. *Numbered curves* represent differentiation paths: 1—differentiation of mafic to intermediate plutons, 2—complementary differentiation trend seen in the pyroxenites, and 3—generation of granitic magmas by partial melting of pre-existing crust. **a** MgO versus SiO_2, **b** total Fe as FeO versus SiO_2, **c** Mg# (molar Mg/(Mg + Fe)) versus SiO_2, **d** Al_2O versus SiO_2, **e** Na_2O versus SiO_2, and **f** CaO versus SiO_2. All concentrations are in weight percent. *Open cross symbol* labeled "BCC" refers to estimate of global average bulk continental crust (Rudnick and Fountain 1995)

1–3 GPa, corresponding to depths between 30–90 km (Table 2), which is consistent with previous studies (Mukhopadhyay and Manton 1994; Ducea and Saleeby 1996, 1998). These equilibration pressures roughly overlap those estimated from garnet-bearing peridotites from the same xenolith suite (Mukhopadhyay and Manton 1994; Ducea and Saleeby 1996, 1998a; Lee et al. 2001). For the low MgO pyroxenites, which do not contain orthopyroxene, we are unable to estimate pressure reliably. Chromium contents are too low in the clinopyroxenes in the low MgO group to use a Cr-in-diopside barometer (Nimis and Taylor 2000).

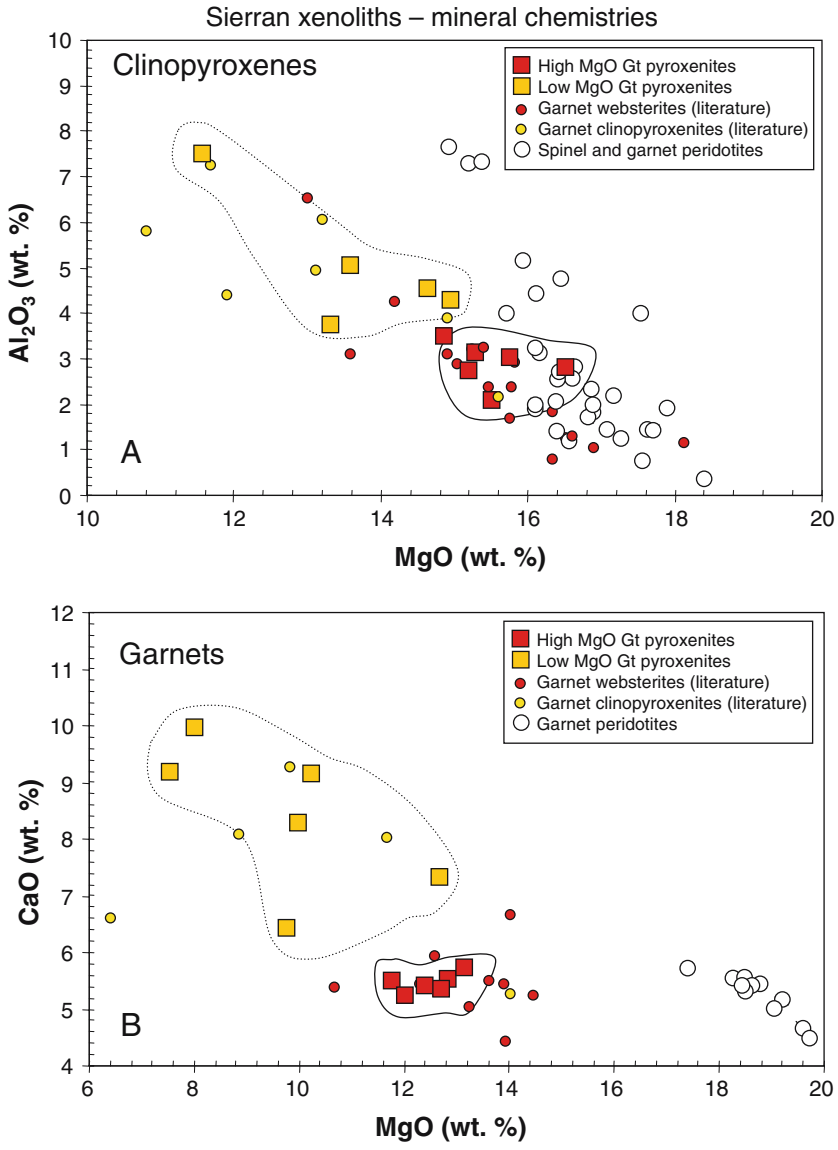

Fig. 3 Mineral chemistries of Sierran xenoliths. **a** Al_2O_3 versus MgO in clinopyroxenes, **b** CaO versus MgO for garnets. *Large squares* represent mineral chemistry data from the samples in this study (Table 2) and are categorized here based on the bulk compositions of the xenoliths from which they derive. Also shown are previously published clinopyroxene and garnet compositions for pyroxenite and peridotite xenoliths from the same xenolith suite (Dodge et al. 1988; Mukhopadhyay and Manton 1994; Lee et al. 2001). Previously published pyroxenite data are classified as either garnet websterites (gt + opx + cpx) or garnet clinopyroxenites, the former corresponding to high MgO pyroxenites and the latter to low MgO pyroxenites

Temperatures for the low MgO garnet pyroxenites, which contain only garnet and clinopyroxene, can be made using thermometers based on Fe–Mg exchange between garnet and clinopyroxene (Ellis and Green 1979). The temperatures last recorded by the low MgO pyroxenites range between 695–831°C (Table 2). For the high MgO pyroxenites, which contain orthopyroxene in addition to garnet and clinopyroxene, temperatures can be estimated using thermometers based on Fe–Mg exchange between two pyroxenes (Wells 1977; Brey and Kohler 1990), garnet and orthopyroxene (Harley 1984), and garnet and clinopyroxene (Ellis and Green 1979). Temperatures calculated as such range between ~500–900°C. We caution that there is considerable mismatch in temperatures calculated based on different equilibria (200°C difference), indicating considerable disequilibrium. For these reasons, we do not feel that any of the subtle differences in temperature between the two pyroxenite groups are robust, and it is not possible to determine if the two pyroxenite groups come from different parts of the Sierran lithosphere based on thermobarometry alone. We are, however, confident that both pyroxenite groups record equilibration temperatures below 900°C. Extensive exsolution textures are probably attributable to cooling. This is consistent with peridotite xenoliths from the same xenolith suite showing zoned mineral chemistries and textures (garnet rimming spinel) indicating cooling from temperatures from at least as high as 1,000°C to temperatures as low as 700°C (Lee et al. 2000; Lee et al. 2001).

Sierran plutons

The Sierra Nevada is dominated by granitic and granodioritic plutons, with mafic plutons (gabbros and diorites) making up less than 5% of the outcrop area of the batholith (Bateman and Chappell 1979; Moore 1987;

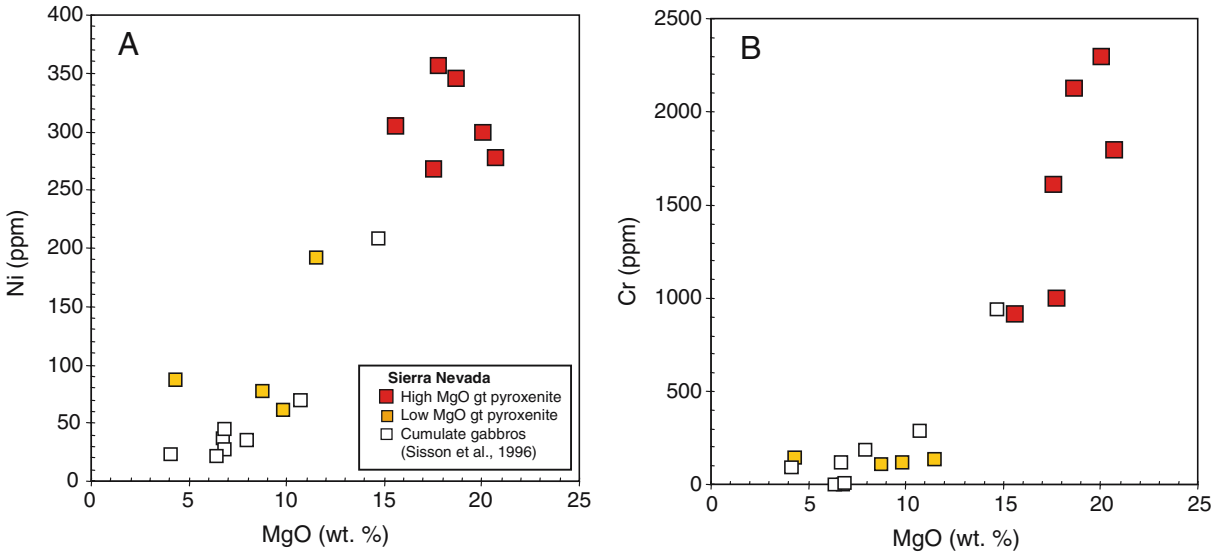

Fig. 4 **a** Ni (ppm) versus MgO (wt. %) in the Sierran garnet pyroxenites (this study) and Sierran cumulate gabbros (Sisson et al. 1996). **b** Cr (ppm) versus MgO (wt. %). Symbols as in Fig. 2

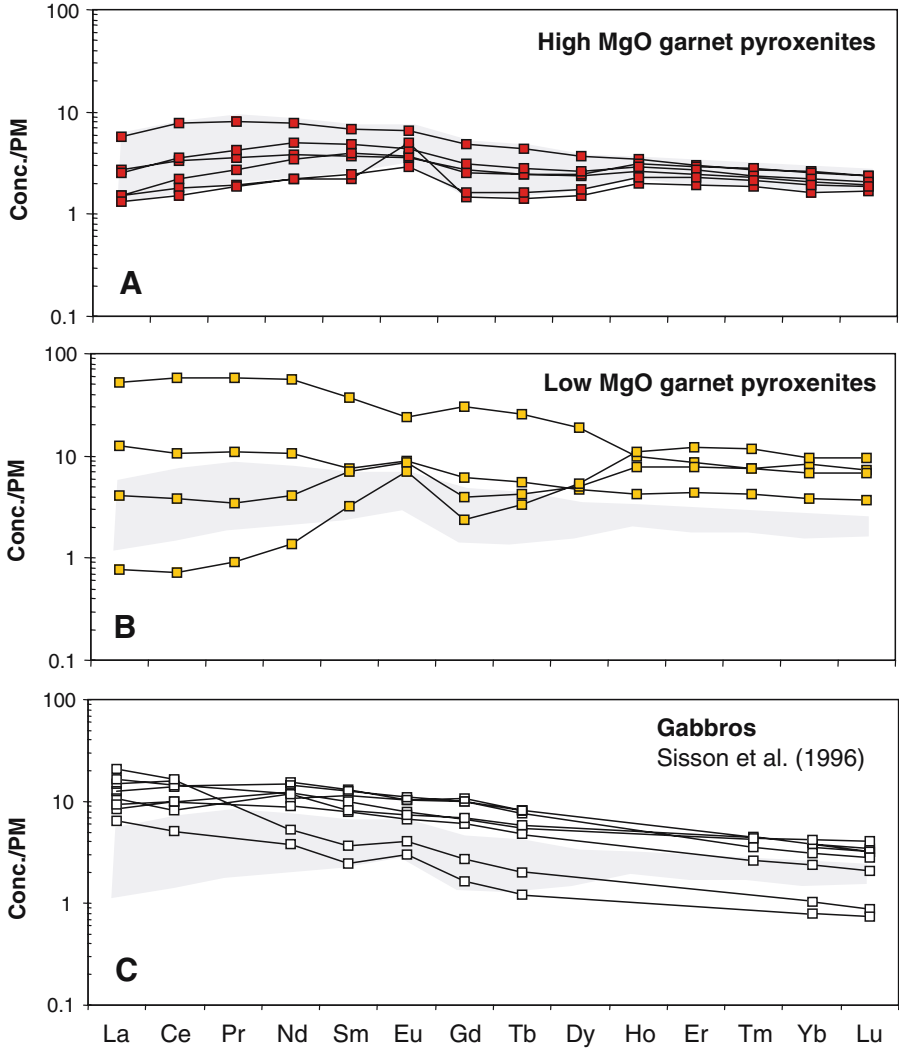

Fig. 5 Primitive-mantle normalized rare-earth element abundance diagrams. **a** High MgO garnet pyroxenites, **b** low Mgo garnet pyroxenites, and **c** Sierran cumulate gabbros (Sisson et al. 1996). *Shaded region* in *a-c* corresponds to the range seen in high MgO garnet pyroxenites (**a**)

Sisson 1992). Although the outcrop area of mafic plutons is small, mafic plutons are widespread in the batholith and small mafic inclusions (enclaves) are found in most plutons at an abundance of several per square meter of outcrop (Barbarin et al. 1989; Sisson et al. 1996). In Fig. 2, a compilation of Sierra Nevadan mafic to felsic plutonic rocks (Peck and Van Kooten 1983; Ague and Brimhall 1988; Bateman et al.1988; Barbarin et al. 1989; Bateman1989; Sisson 1992; Sisson et al. 1996; Ratajeski et al. 2001; Wenner and Coleman 2004) has been plotted for comparison with the garnet pyroxenite xenoliths as discussed above. Mafic and felsic rocks are represented from both west and east of the $^{87}Sr/^{86}Sr_i = 0.706$ line, which is generally taken to represent the transitional boundary from Phanerozoic lithosphere to the west and Precambrian cratonic lithosphere to the east (Kistler and Peterman 1973; Kistler 1990). There has been no attempt to distinguish mafic plutons from enclaves because their FeO, SiO_2, MgO, Al_2O_3 and CaO systematics are very similar.

It can be seen from Fig. 2 that the Sierran magmatic series extend from rather primitive endmembers ($SiO_2 \sim$ 48–55 wt. %), as represented by gabbroic and dioritic plutons and mafic enclaves, to highly evolved endmembers ($SiO_2 \sim$ 60–70 wt. %) as represented by granodiorites, tonalites, and granites. However, an important feature to recognize is that although many of the mafic plutons and enclaves have basaltic to basalt-andesitic bulk compositions in terms of SiO_2 content ($SiO_2 \sim$ 48–55 wt. %), their MgO (4–6 wt. %) contents and Mg#s (0.4–0.5) are much too low to have been directly derived from a peridotitic mantle having Mg#s of 0.88–0.89 (Figs. 2a, c). Magmas derived directly from melting of such peridotite should have Mg#s of ~0.7 and MgO contents typically greater than or equal to 8 wt. % MgO. This can be seen from Figs. 2a, c: the MgO and Mg#s of the mafic Sierran magmas are significantly lower than basaltic lavas from the Cascades arc and mid-ocean ridge basalts at a given SiO_2 content (GEOROC http://www.georoc.mpch-mainz.gwdg.de/georoc/ and RidgePetDB databases (Lehnert et al. 2000). The Cascades arc, which extends from northern California north through Washington, were chosen to serve as an endmember example of an incipient arc where many of the eruptives are basaltic and undoubtedly mantle-derived (Leeman et al. 2005). Sierran mafic magmas also appear to have slightly higher Al_2O_3 for a given SiO_2 content than Cascades basalts (Fig. 2d). Sisson et al. (1996) were the first to point out the unusually low Mg and high Al contents of mafic plutons in their study of the Onion Valley intrusive suite in the high Sierra Nevada. The regional data synthesis presented here indicates that this distinctive geochemical signature is a general feature of nearly all mafic magmas (enclaves and plutons) in the Sierra Nevada. What is clear from the comparison of Sierran mafic plutons to Cascades basalts is that the Sierran mafic plutons, despite their low SiO_2 contents, have experienced more deep level fractionation than have mid-ocean ridge basalts and basalts in young arcs built upon thin pre-existing lithosphere, such as the Cascades. These compositional distinctions will be discussed in the next section.

Discussion

High MgO garnet pyroxenites are cumulates from hydrous basalts or basaltic andesites

We consider four hypotheses for the origin of high MgO garnet pyroxenites: (1) trapped and solidified melts,(2) melt-rock reaction products, (3) solid residues of partial melting, and (4) cumulates.

Hypothesis 1: solidified melt

We begin our discussion by referring to Fig. 2, where major-element compositions of the Sierran garnet pyroxenites are compared to Sierran plutonic rocks and to extrusive rocks in the active Cascades arc (mid-ocean ridge basalts have roughly similar Mg#, MgO, SiO_2 and Al_2O_3 compositions to the primitive Cascades lavas and are hence not plotted). It can be seen that the major element systematics of the high MgO garnet pyroxenites do not match any of the primitive magma compositions shown in the plot. The MgO and Al_2O_3 contents are too high and low, respectively, to represent typical basaltic melts. In particular, the Mg#s (up to 0.82) are much too high to represent any magma observed in the Phanerozoic. Only picrites (basalts that have experienced olivine accumulation) or Archean komatiites can reach Mg#s so high. However, such magmas have low SiO_2 contents because they have either accumulated olivine or are olivine-saturated even at high pressure. The higher SiO_2 and CaO contents of the high MgO pyroxenites compared to any Sierran magma compositions preclude the involvement of olivine accumulation at any point in the history of the high MgO pyroxenites. The Sierran high MgO garnet pyroxenites thus are not solidified melts.

Hypothesis 2: melt-rock reaction

The next hypothesis to consider is the high MgO garnet pyroxenites as melt-rock reaction products. It has been shown on theoretical, observational, and experimental grounds that pyroxene-rich mantle assemblages can be generated by reaction of a silicic melt with peridotite (Sekine and Wyllie 1982; Johnston and Wyllie 1989; Sen and Dunn 1994; Kelemen 1995; Kepezhinskas et al. 1995; Rapp et al. 1999; Liu et al. 2005). Such a scenario might arise if a silicic melt derived from slab melting rises into the hotter mantle wedge. Reaction with a silicic melt would result in the conversion of olivine to pyroxene, generating pyroxenites or pyroxene-rich peridotites. In some cases, garnet would also form if at sufficiently high pressures and/or water fugacities. The

melt, itself, would remain relatively silicic but would have its Mg#, Ni, and Cr contents increased. Natural examples of veined mantle formed by such processes are rare or at least difficult to demonstrate. However, some xenoliths in northeastern China can be unequivocally demonstrated to be melt-rock reaction products because the original reaction "contacts" are preserved in large composite xenoliths (Liu et al. 2005). Such garnet pyroxenites are distinctive in that their Mg#s range continuously from 0.8 to 0.9, overlapping that of primary wallrock peridotite. In addition, the Chinese garnet pyroxenite reaction veins have compositions that point toward conversion of olivine to garnet and pyroxene by reaction with a silicic endmember. None of these features are shown by the Sierran high MgO garnet pyroxenites. Their Mg#s reach a maximum of 0.82, which begs the question of where the intervening Mg#s are if these samples are truly reaction products with peridotites having Mg#s of 0.89 or greater. In addition, we have never observed any composite xenoliths in the xenolith suites. Finally, as pointed out in the previous paragraph and demonstrated in Fig. 2, the Sierran high MgO pyroxenites show little to no compositional evidence for the involvement of olivine in their formation.

Hypotheses 3 and 4: restites and cumulates

We now consider the last two hypotheses, restite and cumulate origins. Cumulate textures have been reported in some of the Sierran garnet pyroxenite xenoliths (Ducea and Saleeby 1996), but in many cases, these samples have recrystallized, obfuscating original igneous textures. For these reasons, we turn to compositional data. We appreciate that distinguishing between restite and cumulate origins based on compositional data alone is notoriously challenging because, in a closed system at equilibrium, cumulates are compositionally indistinguishable from restites for a given melt fraction. However, we can still gain insight by considering what melt fractions are implied by the compositions of the high MgO pyroxenites, allowing us to assess the physical plausibility of the deduced melt fractions. To do so, we begin by considering batch melting (or batch crystallization) experiments for two different starting compositions.

The first starting composition is that of a typical tholeiitic basalt (G2 in Pertermann and Hirschmann 2003a, b; 50.1 wt. % SiO_2, 7.90 wt. % MgO, 9.35 wt. % FeO*, Mg# = 0.60). Plotted in Fig. 6 are experimental melts and reconstructed residues from partial melting

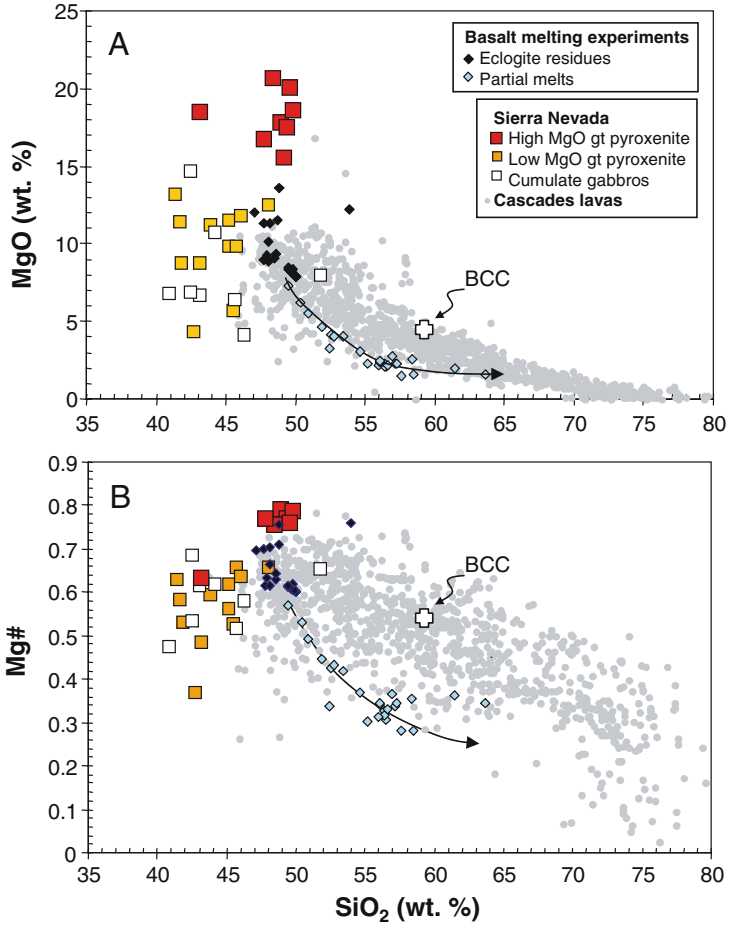

Fig. 6 MgO (**a**) and Mg# (**b**) versus SiO_2, as in Figs. 2a and 2c, respectively. Results of basalt melting experiments in the eclogite stability field (2 and 3 GPa) are shown (Pertermann and Hirschmann 2003a, b). *Gray diamonds*represent partial melts of eclogitized basalt while *black diamonds*represent reconstructed residues of melting. *BCC* bulk continental crust. *Open cross* symbol labeled "BCC" refers to estimate of global average bulk continental crust (Rudnick and Fountain 1995)

experiments of this starting composition at 2 and 3 GPa, wherein garnet and clinopyroxene are stabilized (Pertermann and Hirschmann 2003a, b). Partial melting of "eclogitized" basalt results in silicic melts with lower MgO and Mg# and higher SiO_2 relative to their parent. In contrast, the complementary solid residues trend towards higher MgO and lower SiO_2 contents. However, only under extremely high degrees of melting (>90%) for this particular starting composition (or equivalently, extremely low degrees of crystallization from a magma having a composition equal to the starting composition in these experiments) are the high MgO values characteristic of the high MgO Sierran garnet pyroxenites even approached (Pertermann and Hirschmann 2003a, b). If the high MgO garnet pyroxenites represent restites or cumulates from a typical tholeiitic basalt starting composition, very small fractions of high MgO pyroxenites are implied. However, high MgO garnet pyroxenites are not only abundant in the xenolith population but also derive from pressures between 1 and 3 GPa, corresponding to a ~60 km interval (Table 1). This suggests that the high MgO pyroxenites are volumetrically significant (Dodge et al. 1988; Mukhopadhyay and Manton 1994; Ducea and Saleeby, 1996), hence, it seems unlikely that the high MgO pyroxenites are derived from a typical tholeiitic basalt, regardless of a restite or cumulate origin.

More reasonable cumulate (or restite) fractions arise if we assume instead that the composition of the parental magma (or starting composition) is more Mg-rich, that is, more primitive. An example of a more primitive magma would be one that is more saturated in olivine; such a magma would consequently have higher MgO and lower SiO_2. However, the high SiO_2 contents of the high MgO garnet pyroxenites and the absence of olivine suggests derivation from a pyroxene-saturated magma rather than an olivine-saturated magma. What seems necessary is a parental magma or solid having high MgO content and higher SiO_2. One such composition is a high MgO content basaltic andesite. Müntener et al. (2001) studied the crystallization products of a basaltic andesite from Mount Shasta, California (51.7 wt. % SiO_2, 10.79 wt. % MgO, 7.93 wt. % FeO, and a Mg# of 0.71; Baker et al. 1994) at 1.2 GPa and under hydrous conditions (by adding 3.8 to 5 wt. % H_2O). They showed that such magmas would crystallize clinopyroxene–orthopyroxene (±garnet) assemblages instead of olivine-bearing assemblages due to a decrease in olivine saturation field by a combination of increased pressure and hydrous conditions. The compositions of their crystallization products are shown as crosses in Fig. 2. It can be seen that for all the major elements plotted in Fig. 2, there is a close similarity to the Sierran high MgO garnet pyroxenites. We recognize that the Sierran high MgO garnet pyroxenites have more modal garnet than those of Müntener et al. (2001). However, the Sierran high MgO garnet pyroxenites have already cooled down to temperatures ~700°C, which is at least 300°C lower than the temperatures at which pyroxenite assemblages crystallized in the experiments of Müntener et al. The higher garnet mode in the Sierran high MgO pyroxenites could be due in part to subsolidus exsolution from high temperature, and hence, high Al pyroxenes (this is consistent with the textures described earlier). It is also likely that the Sierran high MgO garnet pyroxenites formed at pressures greater than the experimental pressures of 1.2 GPa (see Sect. 3.1.2) and, as such, would probably have had more garnet on the liquidus (or solidus, if a restite origin is preferred).

If the Sierran high MgO garnet pyroxenites are indeed derived from hydrous basaltic andesite compositions, the implied residual melt fraction (cumulate origin) or partial melting degree of the parent (restite origin) is probably around 50% (Müntener et al., 2001) and hence still high. We also note that significantly lower melt fractions (e.g., <10–20%) are unlikely. These pyroxenites are not residues of small degree melting or cumulates from near-complete crystallization. As pointed out above, the compositions of these high MgO pyroxenites do not approach any typical melt composition. Moreover, low melt fractions are inconsistent with the Ti systematics. Recent rutile solubility experiments have shown that for TiO_2 contents typical of average tholeiitic basalts (e.g., MORB), rutile will be present on and/or slightly above the solidus of eclogite melting, but absent at higher degrees of melting (20%) due to dissolution into the melt (Klemme et al. 2002). However, despite the presence of rutile in the Sierran high MgO pyroxenites, nearly all have very low TiO_2 contents compared to most basaltic magmas, suggesting that rutile may not have been present on the solidus or liquidus. The same conclusion can be drawn from Nb/Ta systematics (Table 3). Sierran high MgO pyroxenites have Nb/Ta ratios overlapping the range seen in arc lavas from the Cascades and elsewhere (Münker et al. 2004), yet if rutile was involved during magmatic petrogenesis, Nb–Ta systematics would have been controlled solely by rutile and low Nb/Ta ratios would be expected for the high MgO pyroxenites (because Nb and Ta are extremely compatible in rutile and, in addition, rutile prefers Ta much more than Nb; (Foley et al. 2002; Rapp et al. 2003; Klemme et al. 2005). These observations indicate that rutile was never involved in the magmatic origin of Sierran high MgO pyroxenites. The rutile currently present in our samples most likely exsolved from pyroxenes and garnet during cooling. More importantly, the lack of rutile hints at fairly large melt fractions, consistent with our interpretation that the high MgO pyroxenites derive from ~50% melting or crystallization of a basaltic andesite.

We are now faced with the question of whether the high MgO pyroxenites are cumulates or restites? Our preferred interpretation is that they are cumulates. This is because if they were restites, we would expect a continuum of compositions ranging from the unmelted parent material to residues that have experienced high degrees of melt extraction. This conclusion is based on the following argument. Consider the physical

Table 3 Whole-rock trace element geochemistry

		BHVO1	BIR1	LOD	AGV1		JP1	BC98-9		BC52	BCX		BC49	BC76		BC41		BC98-5		BC72	BC98-7	BC98-1		
		Calibration values																						
		ppm	ppm	ppm	ppm	ppm	ppm	ppm	ppm	ppm	ppm	ppm	ppm	ppm	ppm	ppm	ppm	ppm	ppm	ppm	ppm	ppm	ppm	ppm
Li	LR-ICPMS	4.9	3.4	0.017	11	12	1.4	8.8	18	18	20	51	21	14	13	13	14	11	14	13	10	10	5.8	13
Be	LR-ICPMS	1.1	0.116	0.012	2.6		0.018	0.95		0.68	0.74		0.48	0.52		0.48		0.27		0.26	0.21	0.36		
Sc	MR-ICPMS	31.8	43.8	0.003	11.0	12.1	7.68	8.06	7.43	48.3	52.8	50.7	63.3	56.9	48.8	55.9	54.6	62.7	58.8	57.1	48.6	43.9	41.8	43.0
	XRF									49	53			45		47		59		53	53	48		
Ti	MR-ICPMS	16,610	6,036	1.337	6,342	6,375	24.87	2,413	2,279	9,910	2,436	2,283	2,313	4,774	5,056	2,872	2,946	3,700	3,576	3,651	2,507	3,104	3,025	2,820
V	MR-ICPMS	321	322	0.017	117	123	28.1	118	112	425	542	497	269	347	358	265	259	294	284	270	233	246	240	265
	XRF							128		429	507			342		281		283		239	214	235		
Cr	MR-ICPMS	289	412	0.557	10.8	NA	2,802	112	98.0	79.0	105	84.1	133	914	NA	991	2,294	1,731	1,517	2,258	2,301	1,963	1.218	NA
Mn	MR-ICPMS	1317	1355	0.049	708.4	784.8	933.5	3552	3618	1760	2139	2071	2370.7	1,144	1,032	1,097	1,128	1,379	1,379	1,255	1,629	1,678	1,617	1,716
Fe	MR-ICPMS	85,542	79,037	2.176	39,810	49,790	59,870	93,800	91,280	99,850	98,560	94,330	100,100	68,500	62,100	64,000	64,680	73,600	71,870	67,940	87,080	92,420	83,470	87,530
Co	LR-ICPMS	45	53	0.018	15.1	16.7	115.7	20.0	16.4	46.5	41.1	37.0	78.4	55.8	51.0	48.4	49.4	54.9	55.3	58.5	70.5	68.5	68.0	69.8
Ni	LR-ICPMS	120	175	0.024	22.8	18.9	2459.2	86.8	56.8	77.8	61.4	47.1	191	305	305	357	343	269	241	345	299	277	257	331
	XRF							52		61	51			278		330		233		328	283	264		
Cu	MR-ICPMS	136	113	0.158	57.2	62.7	4.4	7.7	2.6	108.2	76.4	80.0	192.1	96.2	95.5	77.0	78.2	61.4	62.7	48.9	73.8	66.8	65.8	75.4
	XRF							11		120	88			102		78		65		55	76	69		
Zn	MR-ICPMS	105	65	0.407	86.5	104.0	51.2	54.0	51.0	88.4	155.2	165.1	115.4	61.1	55.2	73.7	66.6	68.1	67.7	56.7	90.2	94.6	100.5	85.8
	XRF							55		85	155			57		71		69		57	82	91		
Ga	LR-ICPMS	21	15.2	0.004	19.5	23.6	0.6	11.5	12.1	15.8	14.0	14.4	11.0	11.0	11.2	8.3	8.8	9.7	9.9	8.6	8.9	11.9	11.2	12.8
	XRF							16		14	18			14		8		14		11	10	15		
Ge	LR-ICPMS		1.5	0.034	1.9		1.2	2.1		3.8	1.8		1.8	1.5		1.4		1.4		1.4	1.5	1.7		
Rb	LR-ICPMS	9.31	0.195	0.015	62.7	74.7	0.027	0.857	1.08	11.1	11.4	11.9	4.11	6.9	13.7	5.42	5.94	1.03	1.58	7.46	2.37	4.29	4.73	6.11
Sr	LR-ICPMS	396	106.4	0.009	658	685	0.548	72.4	74.3	159	136	140	61.0	98.9	122	95.6	101.2	60.6	62.5	63.5	87.5	57.2	59.4	77.8
	XRF							81		173	147			101		104		67		68	93	63		
Y	LR-ICPMS	28	16.2	0.002	18.8	21.1	0.13	21.4	21.1	39.3	34.7	34.4	48.1	14.0	10.7	10.6	11.0	12.8	12.8	11.3	8.55	9.66	8.53	9.01
	XRF							23		40	32			13		11		13		12	8	10		
Zr	LR-ICPMS	181	14.47	0.010	228	253	6.3	56.6	61.7	22.7	25.3	25.9	22.4	49.9	39.6	16.6	17.8	21.3	22.4	21.6	11.2	14.7	14.4	16.3
	ID							56.3		21.7	22.3		15.9	47.3		15.1		18.4		22.2	8.92	13.7		
	XRF							67		32	34			49		22		26		24	15	19		
Nb	LR-ICPMS	18.1	0.558	0.002	13.7	13.9	0.084	0.16	0.15	8.18	1.45	1.43	0.23	2.68	0.79	0.29	0.34	0.22	0.23	0.32	0.30	0.35	0.36	0.35
	XRF							3.4		9.3	3.2			3		2.1		2		1.7	1.3	2.2		
Cs	LR-ICPMS	0.1	0.005	0.001	1.31	1.31	0.042	0.288	0.255	3.14	1.86	1.74	0.373	0.315	0.461	0.293	0.281	0.205	0.188	1.29	0.117	0.947	0.914	0.997
Ba	LR-ICPMS	133	6.52	0.019	1,261	1,214	8.95	14.4	16.0	141	184	188	257	159	283	63.3	46.8	49.6	40.9	65.7	257	61.0	33.3	76.7
Ba	XRF							13		139	186			150		71		61		74	245	63		
La	LR-ICPMS	15.5	0.604	0.002	34.7	39.3	0.039	8.27	8.10	34.4	2.63	2.44	0.49	3.78	3.85	1.76	1.83	0.971	1.01	1.66	0.990	0.863	0.867	1.05
Ce	LR-ICPMS	38	1.897	0.004	66.7	66.0	0.086	17.9	17.7	96.2	6.28	5.96	1.20	13.2	11.2	5.52	5.74	3.68	3.92	5.99	3.01	2.51	2.46	2.72
Pr	LR-ICPMS	5.33	0.378	0.001	8.20	7.96	0.010	2.80	2.72	14.7	0.888	0.823	0.232	2.02	1.92	0.899	0.923	0.700	0.715	1.08	0.494	0.469	0.451	0.564
Nd	LR-ICPMS	24.8	2.38	0.004	31.2	31.2	0.041	13.4	12.7	70.4	5.03	4.56	1.71	9.80	9.24	4.82	4.73	4.24	4.18	6.19	2.74	2.79	2.53	3.24
Sm	LR-ICPMS	6.12	1.117	0.001	5.65	5.63	0.010	3.02	2.82	15.2	2.90	2.70	1.33	2.77	2.47	1.51	1.45	1.58	1.51	1.98	0.901	1.00	0.893	1.08
Eu	LR-ICPMS	2.1	0.524	0.001	3.78	1.87	0.018	1.42	1.39	3.75	1.28	1.19	1.01	1.00	0.851	0.548	0.490	0.573	0.538	0.677	0.708	0.446	0.349	0.408
Gd	LR-ICPMS	6.26	1.85	0.001	7.52	5.14	0.010	3.39	3.58	16.66	2.18	2.50	1.30	2.64	2.52	1.45	1.58	1.37	1.53	1.67	0.799	0.895	0.912	1.30
Tb	LR-ICPMS	0.954	0.379	0.0002	1.13	0.77	0.002	0.54	0.577	2.55	0.424	0.498	0.326	0.428	0.393	0.244	0.274	0.244	0.273	0.279	0.142	0.162	0.168	0.226
Dy	LR-ICPMS	5.3	2.53	0.001	5.74	3.82	0.012	3.14	3.27	12.80	3.35	3.75	3.56	2.52	2.16	1.58	1.74	1.66	1.82	1.76	1.01	1.16	1.17	1.48
Ho	LR-ICPMS	0.99	0.585	0.0003	0.67	0.65	0.004	0.639	0.599	1.48	1.17	1.09	1.64	0.508	0.411	0.396	0.383	0.461	0.440	0.431	0.298	0.343	0.303	0.342
Er	LR-ICPMS	2.56	1.734	0.001	1.79	1.75	0.014	1.90	1.75	3.82	3.46	3.18	5.30	1.34	1.06	1.09	1.08	1.29	1.24	1.17	0.853	0.987	0.874	0.977
Tm	LR-ICPMS	0.34		0.0002	0.25	0.25	0.003	0.283	0.258	0.516	0.516	0.471	0.802	0.182	0.136	0.154	0.150	0.188	0.175	0.163	0.125	0.145	0.126	0.142

Table 3 (Contd.)

		BHVO1	BIR1	LOD	AGV1		JP1	BC98-9		BC52	BCX		BC49	BC76		BC41		BC98-5		BC72	BC98-7	BC98-1	
		Calibration values																					
		ppm	ppm	ppm	ppm	ppm	ppm	ppm	ppm	ppm	ppm	ppm	ppm	ppm	ppm	ppm	ppm	ppm	ppm	ppm	ppm	ppm	ppm
Yb	LR-ICPMS	2.04	1.649	0.001	1.78	1.62	0.018	1.68	1.65	3.74	2.99	2.95	4.17	1.17	0.815	0.920	0.946	1.11	1.10	0.979	0.730	0.842	0.769	0.862
Lu	LR-ICPMS	0.271	0.247	0.0003	0.24	0.22	0.004	0.246	0.250	0.486	0.452	0.464	0.636	0.162	0.108	0.131	0.137	0.162	0.165	0.140	0.112	0.125	0.119	0.123
Hf	LR-ICPMS	4.21	0.562	0.001	4.83	4.60	0.138	1.90	1.82	1.00	0.884	0.804	0.726	1.76	1.39	0.651	0.616	0.845	0.806	0.881	0.432	0.515	0.450	0.536
	ID							2.10		1.11	0.903		0.589	2.060		0.675		0.862		0.992	0.386	0.465		
Ta	LR-ICPMS	1.14	0.041	0.001	0.809	0.779	0.006	0.029	0.025	0.353	0.088	0.078	0.048	0.205	0.060	0.031	0.029	0.025	0.021	0.028	0.023	0.027	0.025	0.019
Tl	LR-ICPMS	0.059		0.003	0.471	0.409	< LOD	0.012	0.014	0.153	0.151	0.124	1.27	0.123	0.175	0.080	0.072	0.235	0.205	0.072	0.082	0.086	0.073	0.107
Pb	LR-ICPMS	2.1	2.97	0.003	17.1	NA	0.037	0.223	NA	1.263	1.53	NA	0.605	0.491	NA	0.737	NA	0.551	NA	0.467	0.413	0.466	NA	NA
Th	LR-ICPMS	1.26	0.03	0.001	6.28	5.65	0.014	1.20	1.11	0.834	0.495	0.450	0.049	0.209	0.188	0.202	0.193	0.060	0.058	0.267	0.019	0.202	0.161	0.222
U	LR-ICPMS	0.42	0.01	0.001	1.90	1.68	0.015	0.779	0.722	0.256	0.242	0.222	0.129	0.082	0.078	0.134	0.132	0.030	0.030	0.109	0.142	0.104	0.104	0.123
Zr/Hf					47.3	55.1	45.8	29.8	34.0	22.6	28.6	32.3	30.9	28.3	28.6	25.4	28.9	25.3	27.8	24.5	26.0	28.6	31.9	30.4
Nb/Ta					17.0	17.9	14.0	5.4	5.9	23.2	16.6	18.5	4.9	13.0	13.1	9.5	11.8	9.1	11.0	11.2	13.0	12.6	14.5	18.0

LR-ICPMS Low resolution ICP-MS, *MR-ICPMS* medium resolution ICPMS, *ID* isotope dilution, *XRF* X-ray fluorescence spectroscopy, *NA* not analyzed, *LOD* limit of detection, < LOD below limit of detection, *ppm* parts per million by weight

conditions necessary for re-melting basaltic lower crust. In order to do so, the lower crust would have to be heated up by underplating or by crustal thickening (the latter followed by radioactive heating). In either case, one would expect temperature gradients into the wall-rock, such that some regions would melt considerably and others less, but since there can be no first order discontinuities in temperature, it follows that there can be no gaps in the observed degree of melting. The Sierran high MgO pyroxenites, however, form a distinct compositional group, far removed from any plausible parental magma protolith.

We conclude that the Sierran high MgO pyroxenites are cumulates from a hydrous basalt or basaltic andesite. This parental magma could have formed by hydrous melting of peridotite in the asthenospheric mantle wedge above the subducting Farallon plate.

Low MgO pyroxenites are cumulates or restites from evolved basaltic compositions

Like the high MgO pyroxenites, the low MgO garnet pyroxenites also do not have major-element compositions matching most known melt compositions. Most melts having low SiO_2 contents should have higher MgO contents and Mg#s, but this is not the case for the low MgO pyroxenites. Their low Mg#s and Ni and Cr contents also suggest that they are not likely to be the reaction products of silicic magmas with peridotite (Kelemen 1995; Kelemen et al. 1998). This leaves a restite and/or a cumulate origin. They cannot, however, be restites/cumulates from a typical tholeiitic basalt. Low pressure (< 1 GPa) restites/cumulates would exhibit olivine control, but the low MgO contents of these pyroxenites preclude the involvement of olivine. The MgO, Al_2O_3, and SiO_2 contents suggest that the low silica mineral controlling most of the compositional variation is instead garnet or plagioclase. Higher pressure (2–3 GPa) restites/cumulates from a tholeiitic magma would result in a slight increase in MgO and a slight decrease in SiO_2 in the solid residue or cumulate as shown in Fig. 6 where we have plotted solid melting residues of 2–3 GPa eclogite melting experiments of Pertermann and Hirschmann (2003a, b). The SiO_2 and MgO contents of the Sierran low MgO pyroxenites are too low to have been derived from tholeiitic parental material.

The Sierran low MgO pyroxenites may instead be cumulates/restites from a more evolved magma. It is noteworthy that their Ni, Cr, and major element compositions are very similar to some Sierran gabbroic plutons and sills, which have been reported to exhibit unequivocal cumulate textures (Sisson et al. 1996). Sierran gabbros have been interpreted by Sisson et al. (1996). to represent cumulates from the mafic to intermediate Sierran plutons (50–60 wt. % SiO_2). Thus, one possibility is that the Sierran low MgO pyroxenites were once represented by the Sierran gabbros but were

metamorphosed into garnet-clinopyroxene assemblages by subsequent increases in pressure and decreases in temperature. However, the flatter HREE abundance patterns and the higher abundances of HREEs in the low MgO garnet pyroxenites compared to the Sierran gabbroic plutons and sills strongly suggests that the garnet presently in these samples had a primary magmatic origin. We interpret these observations to indicate that many of the Sierran low MgO garnet pyroxenites were probably high pressure (> 2–3 GPa) cumulates from an evolved basaltic to basaltic andesitic magma. Alternatively, the low MgO pyroxenties represent the residues of melting pre-existing basaltic lower crust after it had been depressed into the garnet stability field and subsequently heated to partial melting conditions.

The significance of differentiation trends in Sierran mafic to intermediate plutons

It is clear from the chemical variation diagrams in Fig. 2 that granodiorites in the Sierras must be related to the Sierran mafic plutons and enclaves. In all major-element variation diagrams, there is a continuous and smooth differentiation trend linking the mafic to the felsic endmember (granites). In particular, as pointed out earlier, the mafic endmember actually has low Mg and slightly high Al for a given SiO_2 content when compared to extrusive analogs, such as mid-ocean ridge and Cascades arc basalts. The Sierran diorite-granodiorite-tonalite series appear to have inherited the low Mg and high Al signatures, underscoring their genetic relationship with the Sierran mafic plutons and enclaves. Three possibilities, none of which are mutually exclusive, are that (1) the more felsic plutons represent residual liquids from fractional crystallization of a low MgO basaltic parental magma, (2) the felsic plutons represent liquids formed by re-melting pre-existing lower crust having the composition of a low MgO basalt, and (3) the felsic plutons represent mixtures of the low MgO mafic plutons with granitic magmas, produced by melting of pre-existing upper crustal material, such as sediments. Sisson et al. (1996) suggested that Sierran granodiorites were probably formed by mixing between granitic magmas (formed by melting of pre-existing continental crust) with these low Mg, high Al mafic intrusives rather than by continuous fractional crystallization. It has also been shown that the granitic magmas, themselves, could have formed by re-melting of pre-existing ancient crust or by re-melting recent mafic intrusives (Sisson et al. 1996; Ratajeski et al. 2001,2005; Wenner and Coleman 2004).

Of equal importance is how the mafic plutons and enclaves came to be Mg-poor and Al-rich. Sisson et al. (1996) suggested that the parental magmas to these mafic plutons and enclaves must have originally undergone fractional crystallization at greater depths before rising up to mid-crustal levels. They hypothesized that crystallization of primary basaltic magmas at such depths and in the presence of some water would generate pyroxene-rich cumulates due to the decrease in the olivine saturation liquidus surface and the increase in the pyroxene saturation surface with increasing pressure and water content (Grove and Kinzler 1986; Müntener et al. 2001). Although they found little evidence for relict pyroxene in the mafic plutons that they studied, it can be seen that the low MgO and high Al_2O_3 contents of the Sierran mafic plutons (and enclaves) requires the early removal of some component having high MgO contents but having SiO_2 contents similar to that of basalt. The high MgO Sierran garnet pyroxenites, which are rich in pyroxene, satisfy this requirement (Fig. 2a).

The link between garnet pyroxenites and Sierran mafic to intermediate magmas

In the previous section, it was shown that unlike basaltic lavas from mid-ocean ridges and the Cascades arc, the Sierran mafic magmas have Al_2O_3 contents too high and MgO and Mg#s too low to have been derived directly from the mantle. These features cannot be generated by the removal of olivine-rich residues/cumulates because the low SiO_2 content of olivines would drive derivative liquids towards slightly higher SiO_2 contents. In an MgO–SiO_2 plot, this would be manifested as a negative trend as seen in basaltic lavas from mid-ocean ridges and arcs. However, removal of pyroxene-rich components, such as the high MgO garnet pyroxenites, would easily explain the low MgO and high Al_2O_3 signature of the Sierran mafic magmas at a given SiO_2 content because of the high MgO, low Al_2O_3 and similar SiO_2 contents of pyroxenes relative to a parental primary mantle-derived basalt. On an MgO–SiO_2 and Al_2O_3-SiO_2 diagram, removal of high MgO Sierran garnet pyroxenites results in nearly vertical differentiation trajectories (Fig. 2).

We suggest that, after segregation from the mantle, the parental basalt to the Sierran mafic plutons underwent high pressure fractional crystallization (> 1 GPa), wherein pyroxene instead of olivine was the stable liquidus phase. Pyroxene crystallization could have been further enhanced by the presence of water (Müntener et al. 2001). This scenario differs from basaltic lavas from the Cascades and mid-ocean ridges, wherein fractional crystallization appears to have occurred at lower pressures as evidenced by olivine-controlled differentiation trajectories (cf. Leeman et al. 2005). We suggest that the Sierran lithosphere was probably thicker than that presently underlying the Cascades arc, an example of a young incipient arc (active since 35 Ma ago). The thicker lithosphere beneath the Sierras could be due to the Sierra Nevada arc being much more mature than the Cascades—the Sierras were active between 200 and 74 Ma (Bateman et al. 1963). Thus, a thicker lithosphere beneath the Sierras forced mantle-derived magmas to temporarily stall at greater depths (lower crustal or uppermost mantle), allowing for the crystallization of the high MgO garnet pyroxenites. In contrast, a thinner lithosphere beneath the Cascades allows the magmas to

ascend to shallower depths, where the olivine phase field increases.

Crystallization of high MgO garnet pyroxenites should drive the derivative liquid to low Mg and high Al contents at a constant SiO_2 content. As a consequence, the *derivative* liquid would eventually be forced to crystallize cumulates with greater proportions of an aluminous phase and low MgO contents, or if subsequently solidified, it could be re-melted leaving behind restites having such a composition. At lower crustal pressures, low MgO, garnet-rich pyroxenites would form and at mid-crustal pressures olivine-plagioclase-pyroxene gabbros would crystallize. It can be seen that many of the Sierran gabbros and low MgO garnet pyroxenites have low SiO_2, which would then drive later magmatic differentiation towards increasing SiO_2 content (Fig. 2). We suggest that the low MgO garnet pyroxenites probably represent cumulates of the evolving basaltic magma at lower crustal pressures (some could also be restites), whereas the gabbros, some of which contain olivine, represent cumulates of equivalent evolved magmas at mid-crustal pressures where the olivine phase volume has increased and plagioclase instead of garnet is stable.

In conclusion, a two-step differentiation history is suggested, somewhat akin to an earlier model by Arndt and Goldstein (1989). The Sierran plutonic series appears to first decrease in MgO and increase in Al_2O_3 at constant SiO_2. This is then followed by a kink in the differentiation trend wherein derivative magmas are driven towards more silicic compositions with only slight decreases in MgO and Al_2O_3 (Fig. 2). The pyroxenites record a complementary two-step trend: early-formed cumulates are pyroxene-rich (high MgO garnet pyroxenites) and later stage cumulates are garnet-rich or plagioclase-rich depending upon the pressure of crystallization. The Sierran high and low MgO pyroxenites are thus complementary to the mafic to intermediate plutons.

The need for basaltic recharge in crustal level differentiation

One feature that cannot be explained solely by physical removal of pyroxenite cumulates or restites is that, although MgO contents decrease in the Sierran plutonic series, Mg#s remain constant at ~0.45 between 50 to 60 wt. % SiO_2 (Fig. 2c). The decrease in MgO content can be explained, at face value, by removal of the low MgO garnet pyroxenites, but the constancy of Mg# in the Sierran plutons cannot be explained by this process alone. This is because the Sierran low MgO garnet pyroxenites mostly have higher Mg#s (0.5–0.6) than the Sierran plutons, hence fractional crystallization of low MgO Sierran garnet pyroxenites or gabbros alone should drive Sierran plutons towards low Mg#s.

The high Mg#s in Sierran plutons require a mechanism for buffering Mg# during the differentiation process. One possibility is to call upon interaction of evolved melts with peridotitic mantle. For example, proponents of making continental crust by slab melting invoke hybridization of the low Mg# slab melts with the ultramafic mantle wedge, which buffers the Mg# (and Ni contents) at relatively high values (Kelemen 1995; Drummond et al. 1996; Kelemen et al. 1998). However, in the case of the Sierran plutons, most of the magmatic differentiation involving removal of low MgO garnet pyroxenites probably occurred within the crust as there is no intervening mantle wedge to interact with. In addition, those magmas that have been argued to have reacted with the mantle (e.g., high Mg# andesites; Kelemen 1995) have higher Mg#s (>0.6) than the Sierran plutons (0.5).

An alternative hypothesis is to call upon basaltic underplating or recharge. Recharge can be manifested in two ways. In the first way (cumulate scenario), basaltic magma is simultaneously recharged into an evolving magma chamber, which is simultaneously undergoing fractional crystallization. In the second way (restite scenario), basaltic magma is intruded into already pre-existing lower crust. This causes some of the pre-existing crust to re-melt and mix with the underplated magma (this could also be followed by fractional crystallization). The second process is clearly a discontinuous process, but if we integrate the composition over long periods of time (e.g., the lifespan of an arc), both processes can be treated as somewhat continuous. Thus, the mass transport equations describing both processes can be grossly treated in the same way. As a simple demonstration of the underplating/recharge hypothesis, we begin with the assumption that the size of the magma chamber remains constant, that is, the amount of mass leaving the system via crystallization is equal to the amount of replenished magma. It follows that the rate of change in the concentration C of an element in the magma chamber can be expressed as:

$$\frac{dC}{dt} = C_{in}\frac{\dot{M}_{in}}{M} - C_{out}\frac{\dot{M}_{out}}{M} \quad (1)$$

where C_{in} is the concentration in the new magma entering the system, C_{out} is the concentration in the cumulates, $\dot{M}_{in}$ is the rate of replenishment, $\dot{M}_{out}$ is the rate of crystallization, and M is the mass of the magma chamber. In our case, $\dot{M}_{in}$ is assumed to be equal to $\dot{M}_{out}$. If C_{in} and C_{out} are assumed to be constant, then Eq. 1 can be integrated to yield:

$$C(t) = (C_{in} - C_{out})\frac{\dot{M}_{in}}{M_o}t + C_o \quad (2a)$$

where C_o is the initial concentration in the magma chamber. Eq. 2 can be re-expressed in terms of the fraction of material added to the system, $f = \frac{\dot{M}_{in}}{M_o}t$, to yield

$$C(f) = (C_{in} - C_{out})f + C_o \quad (2b)$$

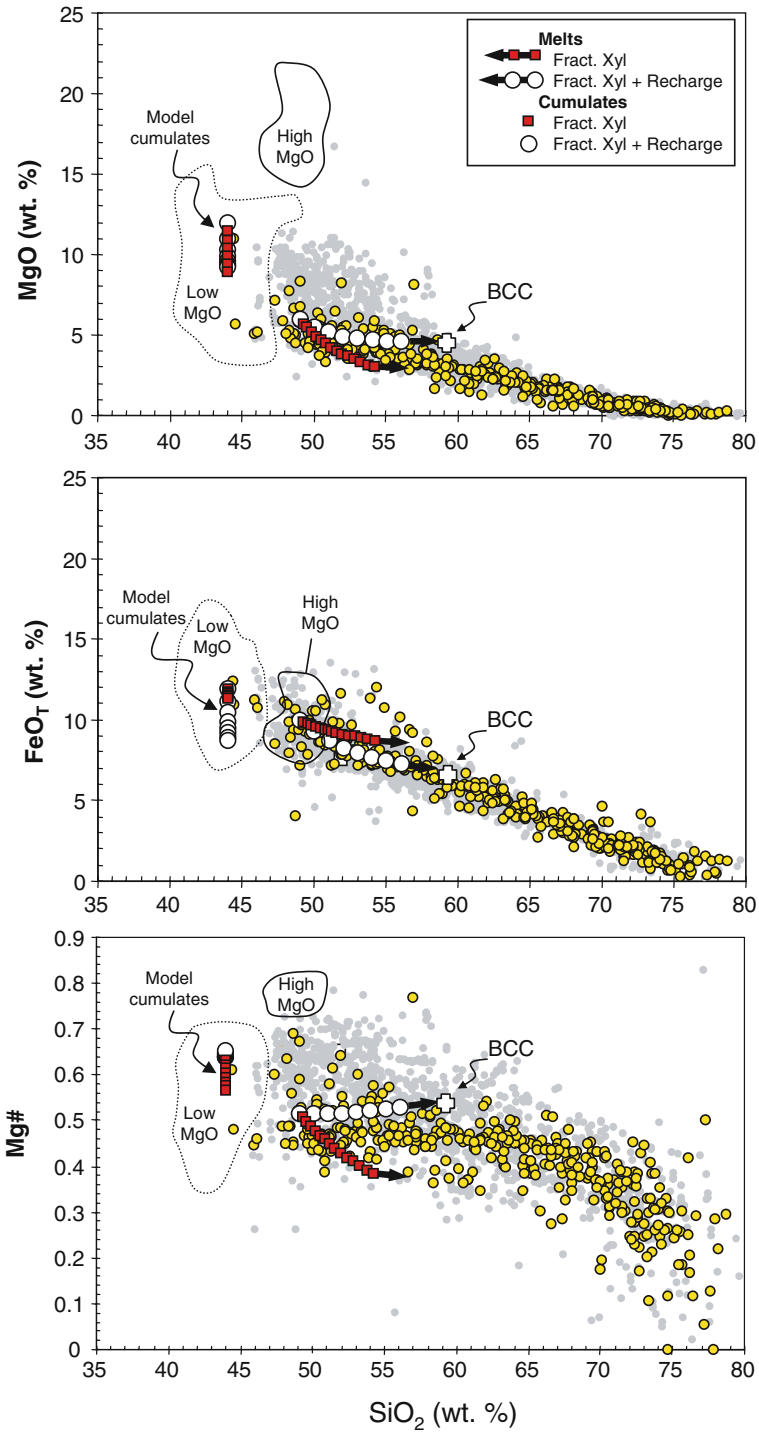

Fig. 7 MgO (**a**), total Fe as FeO (**b**), and Mg# (**c**) versus SiO_2. Symbols as in previous figures. Pure fractional crystallization trends are shown as *curves* with *square symbols*. Fractional crystallization combined with basaltic recharge trends are shown as *curves* with *circle symbols*. The differentiation trends of both magmas and complementary cumulates are shown. Fields of high and low MgO garnet pyroxenites from Fig. 2 are outlined. *Open cross* symbol labeled "BCC" refers to estimate of global average bulk continental crust (Rudnick and Fountain 1995)

On the other hand, if C_{out} is assumed to be related to the concentration of the element in the magma chamber C by a bulk partition coefficient, that is, $C_{out} = DC_{in}$, the solution of Eq. 1 is

$$C(f) = \frac{1}{D}\left(C_{in} - (C_{in} - DC_o)e^{-Df}\right) \quad (3)$$

where we have transformed t into f. Eqs. 2b and 3 give the general relationships for simultaneous crystallization and recharge.

We use Eq. 2b to model the evolution of SiO_2 content and Eq. 3 for MgO and FeO. We assume that the composition of the recharging basalt is similar to that of a primitive mantle-derived basalt (MgO = 9 wt. %, FeO = 8. wt. %, SiO_2 = 49 wt. %). We make the approximation that the SiO_2 contents of the cumulates, as represented by the low MgO garnet pyroxenites and gabbros, remains constant (as represented by the low MgO garnet pyroxenites and gabbros, SiO_2 ~43 wt. %). We assume a bulk D_{MgO} (wt. %) of ~2 and a D_{FeO} of

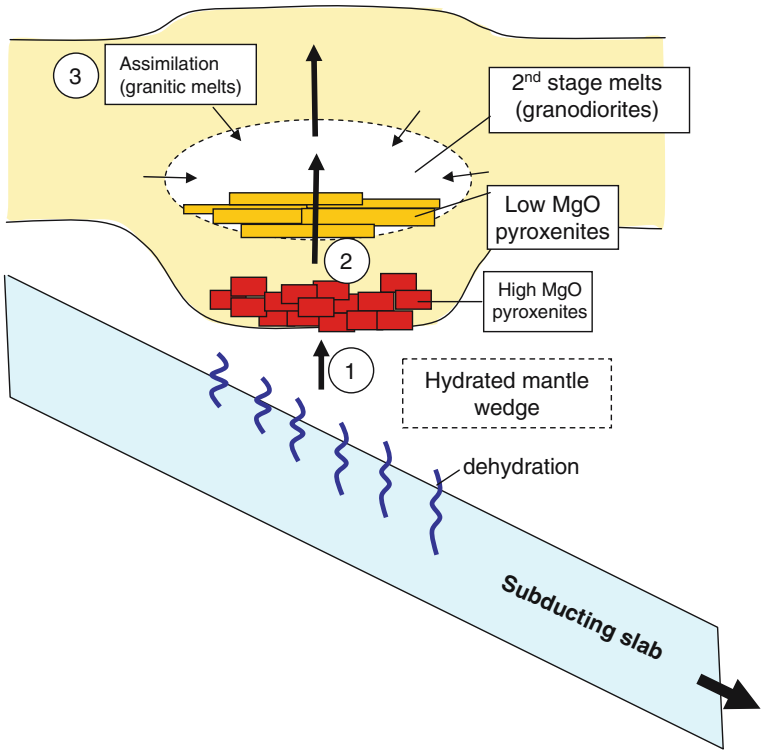

Fig. 8 **a** schematic diagram showing the two-step differentiation process for forming and refining arc continental crust. Step 1 (circle labeled "1"). Hydrous basalts or basaltic andesites are generated in the wet mantle wedge. These magmas (*vertical arrows*) rise to the base of the overriding lithosphere, crystallizing high MgO garnet pyroxenites. Step 2 (*circle* labeled "2"). The derivative melt, e.g., the second stage melt, continues to rise upwards and intrudes into the base of the lower crust. This melt can undergo fractional crystallization, generating low MgO garnet pyroxenite or plagioclase-bearing gabbro cumulates depending on the pressure. Partial melting of country rock might also occur, generating granitic magmas. The composition of the second stage melt evolves as a consequence of fractional crystallization and assimilation of country rock partial melts (final step labeled "3"), the latter of which generates granitic magmas. Superimposed on this two-step scenario is a constant background flux of hydrous basaltic magmatism. Note that Step 2 could also involve re-melting of fully crystallized stage 2 magmas such that the low MgO pyroxenites represent restites instead of cumulates

~1.2. The bulk MgO partition coefficient was estimated from basalt melting experiments (Pertermann and Hirschmann 2003a). The choice of D_{FeO} is higher than that expected for garnet and clinopyroxene, wherein Fe is slightly incompatible. However, to explain the negative correlation between FeO and SiO_2 in the Sierran magma series, the bulk D for FeO and MgO must be greater than 1 (Figs. 7a,b). This is most likely due to the involvement of Fe–Ti oxides during crystallization. Our bulk D_{FeO} was thus chosen so as to fit the FeO–SiO_2 differentiation trend using the simple fractional crystallization (no recharge) and simultaneous crystallization/recharge models (Eq. 3). The FeO- and MgO–SiO_2 differentiation trends are not very sensitive to whether fractional crystallization or simultaneous recharge-crystallization is assumed (Figs. 7a,b). This suggests that our indirect estimate of bulk D_{FeO} is reasonable. However, in contrast to the MgO- and FeO–SiO_2 systematics, the predicted Mg#s of the melt are very sensitive to whether recharge occurs. Without recharge, the Mg#s of the melt drop rapidly, but allowing for basaltic recharge, the Mg# can be maintained at high levels, possibly even increasing slightly (Fig. 7c).

It can be seen that magmatic underplating/recharge can explain the constancy of Mg# in the Sierran plutons. A similar recharge model, albeit at a much smaller scale, has been proposed to explain the compositional evolution of rhyolitic magma chambers in Medicine Lake, northern California (Grove et al. 1997; Kinzler et al. 2000). More sophisticated models can be used to refine this simple model in the future.

An extended model for making and refining crust in continental arcs

In this section, we build on a developing model for the formation and refinement of continental crust in mature arcs (Arndt and Goldstein 1989; Pearcy et al. 1990; Kay and Kay 1993; Rudnick 1995; Tatsumi 2000; Ducea 2002; Kelemen et al. 2003). Hydrous basaltic to basaltic andesite magmas are generated in the mantle wedge overlying a subducting slab (Fig. 8). This magma rises upwards, crystallizing along its way. In the early growth of an arc (incipient arc), the overlying lithosphere is likely to be initially thin, and hence, crystallization

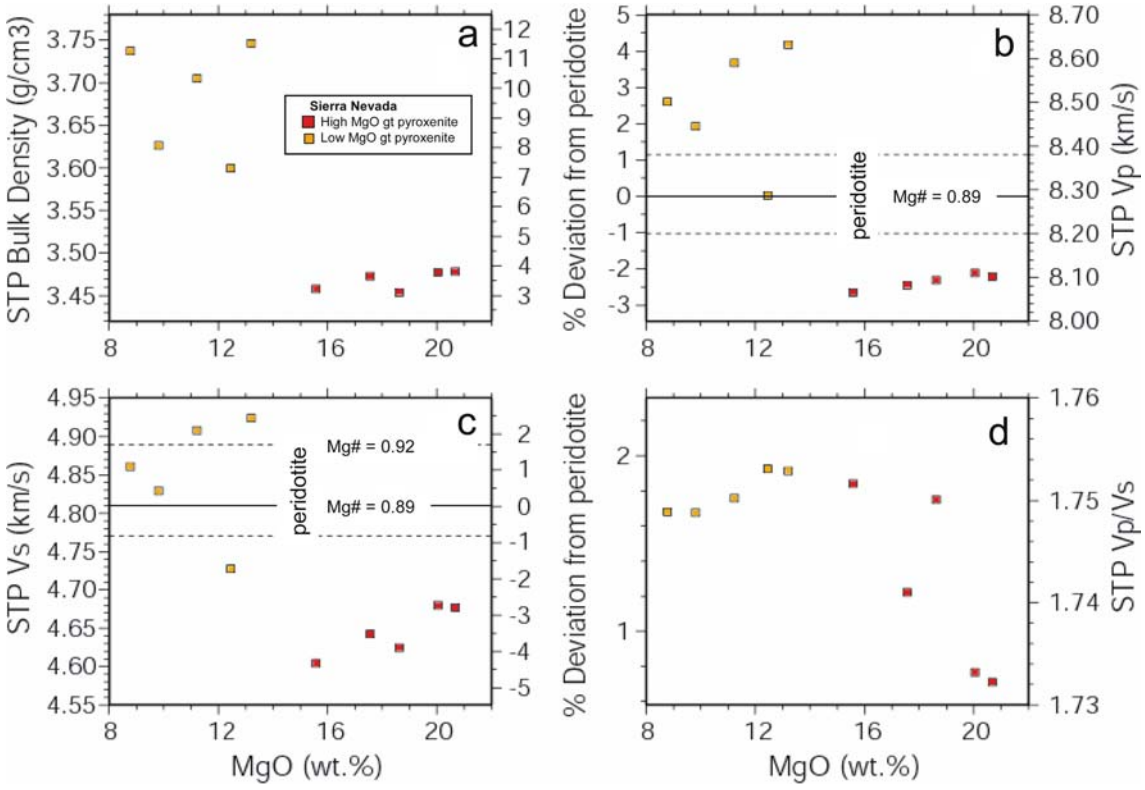

Fig. 9 Densities (**a**), compressional (V_P) and shear wave (V_S) velocities (**b, c**), and V_P/V_S (d) at STP conditions (1 atm, 25°C) for Sierran garnet pyroxenites using data in Table 2 and methods in Lee (2003). *Dashed regions* show range of fertile and residual peridotites thought to make up the bulk of the Earth's upper mantle (Lee 2003).*Solid horizontal line* represents velocities of peridotite corresponding to a Mg# of 0.89. Note that in peridotites V_S correlates with Mg# whereas V_P does not

occurs at shallow pressures where magmatic differentiation involves olivine (as exemplified by the Cascades magmatic arc). However, as the magmatic arc matures (as exemplified by the Sierra Nevada), the crust will thicken, eventually forcing mantle-derived magmas to differentiate at progressively higher pressures, where the olivine saturation surfaces decreases and that of clinopyroxene increases. The higher pressures and the presence of water (Müntener et al. 2001) allow for the crystallization of pyroxene-rich cumulates (with small amounts of garnet) as represented by the high MgO pyroxenites. The derivative magma is consequently driven to low MgO contents without a significant increase in SiO_2. This derivative magma then rises and cools, crystallizing garnet-rich or plagioclase-rich pyroxenites (depending on pressure) having compositions similar to the low MgO garnet pyroxenites. Alternatively, this derivative magma can crystallize completely and be remelted later; in this case, the low MgO pyroxenites would be restites. Regardless of a restite or cumulate origin for the low MgO pyroxenites, basaltic recharge must accompany this part of the differentiation sequence. In the cumulate scenario, fractional crystallization of the second stage magma chamber must be periodically recharged. In the restite scenario, recharge takes the form of basaltic underplating, which melts previously solidified melts and mixes with them.

This two-step process of basaltic differentiation is undoubtedly accompanied by variable extents of partial melting of pre-existing wallrock (Fig. 8). Granitic melts could form from such melting (Ratajeski et al. 2005). These granitic melts will ultimately mix with the mafic magmas interpreted here to derive largely from the addition and differentiation of mantle-derived magmas (Coleman et al. 1992; Coleman and Glazner 1997; Ratajeski et al. 2001). This mixing will contribute to generating the intermediate compositions. Such mixtures of granitic melts derived from ancient crust with more juvenile and primitive magmas will give rise to intermediate magmas having transitional Sr and Nd isotopic signatures as well as non-mantle-like oxygen isotopes (Ducea and Saleeby 1998b). This indirect link between juvenile magma additions and granitoid production has been documented isotopically in other batholiths as well (Holden et al. 1987).

We believe that this two-step differentiation process must eventually be followed by recycling of the pyroxenite layers back into the convecting mantle. The high densities of the Sierran pyroxenites (Fig. 9a) indicate that, once formed, they are likely to "delaminate" on geologically reasonable timescales (Jull and Kelemen 2001). Thus, although the main driving mechanism for basaltic recharge/underplating is the background magmatism associated with hydrous flux

melting in the mantle wedge, this background magmatic flux could be punctuated by magmatic pulses associated with the aftermath of delamination of the mafic pyroxenite layers (Bird 1979; Kay and Kay 1993; Elkins Tanton and Hager 2000). Assuming that the Sierra Nevada batholith has an average MgO and SiO_2 content of ~4 and ~60 wt. % (Fleidner et al. 2000), respectively, and that the parental magma to the mafic to intermediate differentiation series is a basalt to basaltic andesite having MgO and SiO_2 of 9 and 50 wt. %, the amount of complementary high MgO and low MgO pyroxenite collectively is 30–70% of the total parental magma. This flux of material may form important heterogeneities in the Earth's mantle as pointed out by Arndt and Goldstein (1989) and Tatsumi (2000). Such reservoirs could preferentially re-melt due to their low melting temperatures compared to peridotite, contributing to intraplate or mid-ocean ridge magmatism (Hirschmann and Stolper 1996; Kogiso et al. 2003; Pertermann and Hirschmann 2003a, b; Keshav et al. 2004; Sobolev et al. 2005). Some of these "eclogite" reservoirs may be detectable by seismic methods: the low MgO garnet pyroxenites have high compressional and shear wave velocities (Fig. 9b–d) compared to average peridotite (Lee 2003) owing to their high garnet contents. The high MgO garnet pyroxenites have only slightly lower velocities compared to average peridotite and may hence be difficult to detect seismically (Fig. 9b–d).

Acknowledgements The following people are thanked for discussions and/or inspiration relating to the Sierra Nevada, "eclogites", and continental crust over the years: W. P. Leeman, Z.-X. A. Li, R. Rudnick, M. Barth, G. J. Wasserburg, P. Kelemen, E. Humphreys, G. Brimhall, M. Ducea, J. Saleeby, A. Glazner, and G. L. Farmer. Critical reviews by M. Ducea and K. Ratajeski are greatly appreciated and helped to improve the mansucript. Comments made by M. Hirschmann and T. Grove also helped the manuscript. A. Peslier is thanked for help on electron microprobe analyses. This research was supported in part by NSF grants EAR 0440033 and 0309121. Undergraduate support for U. Horodyskyj came from NSF and Rice University.

References

Ague JJ, Brimhall GH (1988) Regional variations in bulk chemistry, mineralogy, and the compositions of mafic and accessory minerals in the batholiths of California. Geol Soc Am Bull 100:891–911

Arndt NT, Goldstein SL (1989) An open boundary between lower continental-crust and mantle-its role in crustal formation and recycling. Tectonophysics 161:201–212

Baker MB, Grove M, Price R (1994) Primitive basalts and andesites from the Mt. Shasta region, N. California: products of varying melt fraction and water content. Contrib Mineral Petrol 118:111–129

Barbarin B, Dodge FCW, Kistler RW, Bateman PC (1989) Mafic inclusions, aggregates and dikes in granitoid rocks, central Sierra Nevada batholith, California – Analytic data. U.S. Geological Survey Bulletin 1899:28

Bateman PC (1989) Bass Lake quadrangle, west-central Sierra Nevada, California - Analytic data. In U.S. Geological Survey Bulletin, vol. B 1809, pp 20

Bateman PC, Chappell BW (1979) Crystallization, fractionation, and solidfiication of the Tuolumne intrusive series, Yosemite National Park, California. Geol Soc Am Bull 90:465–482

Bateman PC, Clark LD, Huber NK, Moore JG, Rinehart CD (1963) The Sierra Nevada batholith: a synthesis of recent work across the central part. In U.S. Geological Survey Professional Paper, vol. 414D, pp 46

Bateman PC, Chappell BW, Kistler RW, Peck DL, Busacca A (1988) Tuolumne Meadows quadrangle, California - analytic data. In U.S. Geological Survey Bulletin, vol. B-1819, pp 33

Bird P (1979) Continental delamination and the Colorado Plateau. J Geophys Res 84:7561–7571

Boyd OS, Jones CH, Sheehan AF (2004) Foundering lithosphere imaged beneath the southern Sierra Nevada, California, USA. Science 305:660–662

Brey GP, Kohler T (1990) Geothermobarometry in four-phase lherzolites II. New thermobarometers, and practical assessment of existing thermobarometers. J Petrol 31:1353–1378

Coleman DR, Glazner AF (1997) The Sierra crest magmatic event: rapid formation of juvenile crust during the Late Cretaceous in California. Int Geol Rev 39:768–787

Coleman DR, Frost TP, Glazner AF (1992) Evidence from the Lamarck Granodiorite for rapid Late Cretaceous crust formation in California. Science 258:1924–1926

Conrad CP, Molnar P (1997) The growth of Rayleigh-Taylor-type instabilities in the lithosphere for various rheological and density structures. Geophys J Inter 129:95–112

DeBari SM, Sleep NH (1991) High-Mg, low-Al bulk composition of the Talkeetna island arc, Alaska: implications for primary magmas and the nature of arc crust. Geol Soc Am Bull 103:37–47

Dodge FCW, Lockwood JP, Calk LC (1988) Fragments of the mantle and crust beneath the Sierra Nevada batholith: xenoliths in a volcanic pipe near Big Creek, California. Geol Soc Am Bull 100:938–947

Drummond MS, Defant MJ, Kepezhinskas PK (1996) Petrogenesis of slab-derived trondhjemite-tonalite-dacite/adakite magmas. Trans Roy Soc Edinburgh 87:205–215

Ducea M (2001) The California arc: thick granitic batholiths, eclogitic residues, lithosphere-scale thrusting, and magmatic flare-ups. Geol Soc Am Today 11:4–10

Ducea MN (2002) Constraints on the bulk composition and root foundering rates of continental arcs: a California arc perspective. J Geophys Res 107: doi:10.1029/2001JB000643

Ducea MN, Saleeby JB (1996) Buoyancy sources for a large, unrooted mountain range, the Sierra Nevada, California: evidence from xenolith thermobarometry. J Geophys Res 101:8229–8244

Ducea MN, Saleeby JB (1998a) Crustal recycling beneath continental arcs: silica-rich glass inclusions in ultramafic xenoliths from the Sierra Nevada, California. Earth Planet Sci Lett 156:101–116

Ducea MN, Saleeby JB (1998b) The age and origin of a thick mafic-ultramafic keel from beneath the Sierra Nevada batholith. Contrib Mineral Petrol 133:169–185

Eggins SM, Woodhead JD, Kinsley L, Mortimer GE, Sylvester P, McCulloch MT, Hergt JM, Handler MR (1997) A simple method for the precise determination of >40 trace elements in geological samples by ICP-MS using enriched isotope internal standardisation. Chem Geol 134:311–326

Elkins Tanton LT, Hager BH (2000) Melt intrusion as a trigger for lithospheric foundering and the eruption of the Siberian flood basalt. Geophys Res Lett 27:3937–3940

Ellis DJ, Green EH (1979) An experimental study of the effect of Ca upon garnet-clinopyroxene Fe-Mg exchange equilibria. Contrib Mineral Petrol 66:13–22

Farmer GL, Glazner AF, Manley CR (2002) Did lithospheric delamination trigger late Cenozoic potassic volcanism in the southern Sierra Nevada, California Geol Soc Am Bull 114:754–768

Fleidner MM, Klemperer SL, Christensen NI (2000) Three-dimensional seismic model of the Sierra Nevada arc, California, and its implications for crustal and upper mantle composition. J Geophys Res 105:10899–10921

Fliedner MM, Klemperer SL (1999) Structure of an island-arc: wide-angle seismic studies in the eastern Aleutian Islands, Alaska. J Geophys Res 104:10667–10694

Foley SF, Tiepolo M, Vannucci R (2002) Growth of early continental crust controlled by melting of amphibolite in subduction zones. Nature 417:837–840

Grove TL, Kinzler RJ (1986) Petrogenesis of andesites. Ann Rev Earth Planet Sci 14:417–454

Grove TL, Donnelly-Nolan JM, Housh T (1997) Magmatic processes that generated the rhyolite of Glass Mountain, Medicine Lake volcano, N. California Contrib Mineral Petrol 127:205–223

Harley SL (1984) An experimental study of the partitioning of Fe and Mg between garnet and orthopyroxene. Contrib Mineral Petrol 86:359–373

Harley SL, Green DH (1982) Garnet-orthopyroxene barometry for granulites and peridotites. Nature 300:697–701

Hirschmann MM, Stolper E (1996) A possible role for garnet pyroxenite in the origin of the "garnet signature" in MORB. Contrib Mineral Petrol 124:185–208

Hofmann AW (1988) Chemical differentiation of the Earth: the relationship between mantle, continental crust, and oceanic crust. Earth Planet Sci Lett 90:297–314

Holden P, Halliday AN, Stephens WE (1987) Neodymium an dstrontium isotope content of microdiorite enclaves points to mantle input to granitoid production. Nature 330:53–56

Johnston AD, Wyllie PJ (1989) The system tonalite-peridotite-H_2O at 30 kbar, with applications to hybridization in subduction zone magmatism. Contrib Mineral Petrol (102)

Jones CH, Kanamori H, Roecker SW (1994) Missing roots and mantle "drips": Regional Pn and telseismic arrival times in the southern Sierra Nevada and vicinity, California J Geophys Res 99:4567–4601

Jull M, Kelemen P (2001) On the conditions for lower crustal convective instability. J Geophys Res 106:6423–6446

Kay RW, Kay SM (1988) Crustal recycling and the Aleutian arc. Geochim Cosmochim Acta 52:1351–1359

Kay RW, Kay SM (1993) Delamination and delamination magmatism. Tectonophysics 219:177–189

Kelemen PB (1995) Genesis of high Mg# andesites and the continental crust. Contrib Mineral Petrol 120:1–19

Kelemen PB, Hart SR, Bernstein S (1998) Silica enrichment in the continental upper mantle via melt/rock reaction. Earth Planet Sci Lett 164:387–406

Kelemen PB, Hanghoj K, Greene AR (2003) One view of the geochemistry of subduction-related magmatic arcs, with an emphasis on primitive andesite and lower crust. Treatise Geochem 3:593–659

Kepezhinskas PK, Defant MJ, Drummond MS (1995) Na metasomatism in the island-arc mantle by slab melt-peridotite interaction: evidence from mantle xenoliths in the North Kamchatka Arc. J Petrol 36:1505–1527

Keshav S, Gudfinnsson GH, Sen G, Fei Y (2004) High-pressure melting experiments on garnet clinopyroxenite and the alkalic to tholeiitic transition in ocean-island basalts. Earth Planet Sci Lett 223:365–379

Kinzler RJ, Donnelly-Nolan JM, Grove TL (2000) Late Holocene hydrous mafic magmatism at the Paint Pot Crater and Callahan flows, Medicine Lake Volcano, N. California and the influence of H_2O in the generation of silicic magmas. Contrib Mineral Petrol 138:1–16

Kistler RW (1990) Two different lithosphere types in the Sierra Nevada, California. In: Anderson JL(ed), The nature and origin of Cordilleran magmatism, vol 174. Geol Soc Am Mem, Geological Society of America, pp. 271–281.

Kistler RW, Peterman ZE (1973) Variations in Sr, Rb, K, Na, and initial Sr^{87}/Sr^{86} in Mesozoic granitic rocks and intruded wall rocks in central California. Geol Soc Am Bull 84:3489–3512

Klemme S, Blundy JD, Wood BJ (2002) Experimental constraints on major and trace element partitioning during partial melting of eclogite. Geochim Cosmochim Acta 66:3109–3123

Klemme S, Prowatke S, Hametner K, Günther D (2005) Partitioning of trace elements between rutile and silicate melts: implications for subduction zones. Geochim Cosmochim Acta 69:2361–2371

Kogiso T, Hirschmann MM, Frost DJ (2003) High-pressure partial melting of garnet pyroxenite: possible mafic lithologies in the source of ocean island basalts. Earth Planet Sci Lett 216:603–617

Lee C-T, Rudnick RL, Brimhall GH (2001) Deep lithospheric dynamics beneath the Sierra Nevada during the Mesozoic and Cenozoic as inferred from xenolith petrology. Geochem. Geophys. Geosys. 2: 2001GC000152

Lee C-T, Yin Q-Z, Rudnick RL, Chesley JT, Jacobsen SB (2000) Osmium isotopic evidence for Mesozoic removal of lithospheric mantle beneath the Sierra Nevada, California. Science 289:1912–1916

Lee C-TA (2002) Platinum-group element geochemistry of peridotite xenoliths from the Sierra Nevada and the Basin and Range, California. Geochim Cosmochim Acta 66:3987–4005

Lee C-TA (2003) Compositional variation of density and seismic velocities in natural peridotites at STP conditions: implications for seismic imaging of compositional heterogeneities in the upper mantle. J Geophys Res 108:2441, doi:10.1029/2003JB002413

Lee C-TA (2005) Trace element evidence for hydrous metasomatism at the base of the North American lithosphere and possible association with Laramide low-angle subduction. J Geol 113:673–685

Leeman WP, Lewis JF, Evarts RC, Conrey RM, Streck MJ (2005) Petrologic constraints on the thermal structure of the southern Washington Cascades. J Volcanol Geotherm Res 140:67–105

Lehnert K, Su Y, Langmuir CH, Sarbas B, Nohl U (2000) A global geochemical database structure for rocks. Geochem Geophys Geosyst 1: 1999GC000026

Liu Y, Shan G, Lee C-TA, Hu S, Liu X, Yuan H (2005) Melt-peridotite interactions: links between garnet pyroxenite and high-Mg# signature of continental crust. Earth Planet Sci Lett 234:39–57

Manley CR, Glazner AF, Farmer GL (2000) Timing of volcanism in the Sierra Nevada of California; evidence for Pliocene delamination of the batholithic root? Geology 28:811–814

Miller DJ, Christensen NI (1993) Seismic signature and geochemistry of an island arc: a multidisciplinary study of the Kohistan accreted terrane, northern Pakistan. J Geophys Res 99:11623–11642

Moore JG (1987) Mount Whitney quadrangle, Inyo and Tulare counties, California - analytic data. U.S. Geological Survey Bulletin 1760

Morency C, Doin M-P (2004) Numerical simulations of the mantle lithosphere delamination. J Geophys Res 109: doi:10.1029/2003JB002414

Mukhopadhyay B, Manton WI (1994) Upper mantle fragments from beneath the Sierra Nevada batholith-partial fusion, fractional crystallization and metasomatism in subduction-related ancient lithosphere. J Petrol 35:1418–1450

Münker C, Wörner G, Yogodzinski G, Churikova T (2004) Behaviour of high field strength elements in subduction zones: constraints from Kamchatka - Aleutian arc lavas. Earth Planet Sci Lett 224:275–293

Müntener O, Kelemen PB, Grove TL (2001) The role of H_2O during crystallization of primitive arc magmas under uppermost mantle conditions and genesis of igneous pyroxenites: an experimental study. Contrib Mineral Petrol 141:643–658

Nimis P, Taylor WR (2000) Single clinopyroxene thermobarometry for garnet peridotites. Part I. Calibration and testing of a Cr-in-Cpx barometer and an enstatite-in-Cpx thermometer. Contrib Mineral Petrol 2000:541–554

Pearcy LG, DeBari SM, Sleep NH (1990) Mass balance calculations for two sections of island arc crust and implications for the formation of continents. Earth Planet Sci Lett 96:427–442

Peck DL, Van Kooten GK (1983) Merced Peak Quadrangle, central Sierra Nevada, California - Analytic data. In U. S. Geological Survey Professional Paper, vol. 1170-D, pp 29

Pertermann M, Hirschmann MM (2003a) Anhydrous partial melting experiments on MORB-like eclogite: phase relations, phase compositions and mineral-melt partitioning of major elements at 2–3 GPa. J Petrol 44:2173–2201

Pertermann M, Hirschmann MM (2003b) Partial melting experiments on a MORB-like pyroxenite between 2 and 3 GPa: constraints on the presence of pyroxenites in basalt source regions. J Geophys Res 108: 10.1029/2000JB000118, 1–17

Rapp RP, Shimizu N, Norman MD (2003) Growth of early continental crust by partial melting of eclogite. Nature 425:605–609

Rapp RP, Shimizu N, Norman MD, Applegate GS (1999) Reaction between slab-derived melts and peridotite in the mantle wedge: experimental constraints at 3.8 GPa. Chem Geol 160:335–356

Ratajeski K, Glazner AF, Miller BV (2001) Geology and geochemistry of mafic to felsic plutonic rocks in the Cretaceous intrusive suite of Yosemite Valley, California. Geol Soc Am Bull 113:1486–1502

Ratajeski K, Sisson TW, Glazner AF (2005) Experimental and geochemical evidence for derivation of the El Capitan Granite, California, by partial melting of hydrous gabbroic lower crust. Contrib Mineral Petrol 149:713–734

Rudnick RL (1995) Making continental crust. Nature 378:571–578

Rudnick RL, Fountain DM (1995) Nature and composition of the continental crust: a lower crustal perspective. Rev Geophys 33:267–309

Seber D, Barazangi M, Ibenbrahim A, Demnati A (1996) Geophysical evidence for lithospheric delamination beneath the Alboran Sea and Rif-Betic mountains. Nature 379:785–790

Sekine T, Wyllie PJ (1982) The system granite-peridotite-H_2O at 30 kbar, with applications to hybridization in subduction zone magmatism. Contrib Mineral Petrol 81:190–202

Sen C, Dunn T (1994) Dehydration melting of a basaltic composition amphibolite at 1.5 and 2.0 GPa: implications for the origin of adakites. Contrib Mineral Petrol 117:394–409

Sisson TW (1992) Triple Divide Peak quadrangle, Fresno and Tulare counties, California - analytic data. U.S. Geological Survey Bulletin 2026

Sisson TW, Grove TL, Coleman RG (1996) Hornblende gabbro sill complex at Onion valley, California, and a mixing origin for the Sierra Nevada batholith. Contrib Mineral Petrol 126:81–108

Sobolev AV, Hofmann AW, Sobolev SV, Nikogosian IK (2005) An olivine-free mantle source of Hawaiian shield basalts. Nature 434:590–597

Tatsumi Y (2000) Continental crust formation by crustal delamination in subduction zones and complementary accumulation of the enriched mantle I component in the mantle. Geochem Geophys Geosys 1: 2000GC000094

Wells PRA (1977) Pyroxene thermometry in simple and complex systems. Contrib Mineral Petrol 62:129–139

Wenner JM, Coleman DS (2004) Magma mixing and Cretaceous crustal growth: geology and geochemistry of granites in the central Sierra Nevada batholith, California. Inter Geol Rev 46:880–903

Wernicke B, Clayton R, Ducea M, Jones CH, Park S, Ruppert S, Saleeby J, Snow JK, Squires L, Fliedner M, Jiracek G, Keller R, Klemperer S, Luetgert J, Malin P, Miller K, Mooney W, Oliver H, Phinney R (1996) Origin of high mountains in the continents: the southern Sierra Nevada. Science 271:190–193

Zandt G, Carrigan CR (1993) Small-scale convective instability and upper mantle viscosity under California. Science 261:460–463

Zandt G, Gilbert H, Owens TJ, Ducea M, Saleeby J, Jones CH (2004) Active foundering of a continental arc root beneath the southern Sierra Nevada in California. Nature 431:41–46